NASA Technical Memorandum 102501
Revised Copy

Review and Statistical Analysis of the Ultrasonic Velocity Method for Estimating the Porosity Fraction in Polycrystalline Materials

D.J. Roth
National Aeronautics and Space Administration
Lewis Research Center
Cleveland, Ohio

D.B. Stang
Sverdrup Technology, Inc.
Lewis Research Center Group
Brook Park, Ohio

S.M. Swickard
National Aeronautics and Space Administration
Lewis Research Center
Cleveland, Ohio

M.R. DeGuire
Case Western Reserve University
Cleveland, Ohio

July 1990

REVIEW AND STATISTICAL ANALYSIS OF THE ULTRASONIC VELOCITY METHOD FOR ESTIMATING THE POROSITY FRACTION IN POLYCRYSTALLINE MATERIALS

D.J. Roth
National Aeronautics and Space Administration
Lewis Research Center
Cleveland, Ohio 44135

D.B. Stang
Sverdrup Technologies, Inc.
NASA Lewis Research Center Group
Cleveland, Ohio 44135

S.M. Swickard
National Aeronautics and Space Administration
Lewis Research Center
Cleveland, Ohio 44135

M.R. DeGuire
Case Western Reserve University
Cleveland, Ohio 44106

E-5298

SUMMARY

A review and statistical analysis of the ultrasonic velocity method for estimating the porosity fraction in polycrystalline materials is presented. Initially, a semi-empirical model is developed showing the origin of the linear relationship between ultrasonic velocity and porosity fraction. Then, from a compilation of data produced by many researchers, scatter plots of velocity versus percent porosity data are shown for Al_2O_3, CuO, MgO, porcelain-based ceramics, PZT, SiC, Si_3N_4, steel, tungsten, UO_2, $(U_{0.30}Pu_{0.70})C$, and $YBa_2Cu_3O_{7-x}$. Linear regression analysis produced predicted slope, intercept, correlation coefficient, level of significance, and confidence interval statistics for the data. Velocity values predicted from regression analysis for fully-dense materials are in good agreement with those calculated from elastic properties.

INTRODUCTION

The physical behavior of components manufactured from polycrystalline materials is in many cases directly dependent on the porosity fraction (volume fraction of pores). As examples concerning key properties of technologically-important materials, porosity fraction has been shown to affect: (1) the strength, toughness and modulus of structural and refractory materials such as steel (ref. 1), tungsten (ref. 2), SiC (ref. 3), Si_3N_4 (ref. 3), and Al_2O_3 (ref. 3), (2) the strength of nuclear fuel materials such as UO_2 (refs. 4 and 5), (3) the thermal shock behavior and strength of porcelain-based ceramics (refs. 6 and 7), (4) the dielectric and elastic properties of piezoelectric materials such as PZT (ref. 8), and (5) the critical current density, diamagnetic response, and modulus of superconducting ceramics such as $YBa_2Cu_3O_{7-x}$ (refs. 9 to 11). In the latter case, reference 9 has shown that porosity

fraction variations on the order of 1 percent in $YBa_2Cu_3O_{7-x}$ samples can result in an order of magnitude variation in critical current density. In such cases where physical properties are directly dependent on porosity fraction, the measurement of porosity fraction becomes important in the quality assurance process for the material.

Currently, various methods are available for measuring the porosity fraction of polycrystalline materials. The most common include dry-weight dimensional and liquid immersion (ref. 12). Other methods for obtaining porosity fraction include estimates from optical areal analysis measurements (ref. 13) and estimates from x-ray attenuation measurements (ref. 14). The choice of method is dependent on experimental conditions including sample geometry and whether additional investigation is required with the sample. For example, the dry-weight dimensional method can only be used for regularly-shaped samples with uniform dimensions such as cubes and rods, while liquid immersion is potentially destructive due to liquid infusion into the sample. Because of the lack of a truly universal porosity fraction measurement method, it seems worthwhile to consider additional measurement/estimation methods that may be useful and convenient in certain laboratory and industrial situations. In this study, we consider the ultrasonic velocity measurement method for estimating porosity fraction.

Ultrasonic velocity is a relatively simple measurement that requires the material specimen to have one pair of sides flat and parallel (ref. 15). The advantages of this method are that it is nondestructive and measurements can be made on different regions of a single specimen. Smith (ref. 2) and Nagarajan (ref. 16) were two of the first researchers to establish empirical correlations between porosity fraction and ultrasonic velocity for polycrystalline materials. The correlations appeared relatively linear over the porosity fraction ranges investigated. Smith's work concerned metallic samples while Nagarajan's work concerned ceramic samples. Other researchers began to investigate similar correlations with different materials. Here, we review and statistically analyze these empirical correlations between ultrasonic velocity and porosity fraction for polycrystalline materials. Initially, a semi-empirical model is developed showing the origin of the linear relationship between ultrasonic velocity and porosity fraction. Then, scatter plots of velocity versus percent porosity data are shown for Al_2O_3, CuO, MgO, porcelain-based ceramics, PZT, SiC, Si_3N_4, steel, tungsten, UO_2, $(U_{0.30}Pu_{0.70})C$, and $YBa_2Cu_3O_{7-x}$. Linear regression analysis produced predicted slope, intercept, correlation coefficient, level of significance, and confidence interval statistics for the data. Additionally, velocity values predicted from regression for fully-dense materials are compared with those calculated from elastic properties.

SEMI-EMPIRICAL MODEL

When there are no boundary effects present, the velocity of a longitudinal ultrasonic wave traveling in a solid is related to the elastic properties and density of the solid by (ref. 17):

$$V = \{[E(1 - \nu)]/[\rho(1 + \nu)(1 - 2\nu)]\}^{1/2} \qquad (1)$$

where V, E, ρ, and ν are the velocity, elastic modulus, bulk density, and Poisson's ratio, respectively, of the material. (The velocity of a shear ultrasonic wave traveling in a solid is related to the elastic properties and density of the solid by:

$$V = \{E/[2\rho(1 + \nu)]\}^{1/2} \qquad (1(a))$$

An "apparent" modulus (ref. 3) for porous materials can be considered which depends on the porosity fraction.

Several early empirical investigations provided evidence that the modulus increases exponentially with decreasing porosity fraction according to (refs. 18 and 19):

$$E = E_o \exp(-bP') \qquad (2)$$

where E_o is the elastic modulus of a fully-dense (nonporous) material, b is an empirically-determined constant related to pore shape, pore distribution, and the ratio of open-to-closed pores, and P' is the porosity fraction. The use of equation (2) to evaluate E_o by extrapolation from fitted experimental data has sometimes resulted in large discrepancies between the extrapolated and observed values (ref. 20). An alternative to equation (2) has been suggested to describe the relationship between elastic modulus and porosity fraction (ref. 21):

$$E = E_o(1 - P')^{2n+1} \qquad (3)$$

where n, like b, is an empirically-determined constant that depends on pore distribution and pore geometry factors.[1]

Porosity fraction, P', can be expressed as:

$$P' = (1 - (\rho/\rho_o)) \qquad (4)$$

where ρ_o is the theoretical (nonporous material) density. Rearranging equation (4) allows us to express bulk density as a function of porosity fraction:

$$\rho = \rho_o(1 - P') \qquad (5)$$

Substituting equations (3) and (5) into equation (1) allows velocity to be expressed as:

$$V = V_o(1 - P')^n \qquad (6)$$

where V_o is a constant for a given material equal to:

$$V_o = \{[E_o(1 - \nu)]/[\rho_o(1 + \nu)(1 - 2\nu)]\}^{1/2} \qquad (7)$$

V_o is the velocity in a fully-dense (nonporous) material, i.e., the "theoretical" velocity. (For shear waves:

$$V_o = \{E_o/[2\rho_o(1 + \nu)]\}^{1/2} \qquad (7(a))$$

The general case for all n can be shown by expanding the right-hand side of equation (6) using the binomial theorem (ref. 22) so that:

$$V = V_o\{1 + [n(-P')] + [n(n - 1) \times (-P')^2/2!] + \ldots + [n(n - 1) \times \ldots (n - k + 1)(-P')^k/k!] + \ldots\} \qquad (8)$$

From the ratio test, equation (8) is absolutely convergent for $|P'| < 1$.

Setting $n = 1$ in equations (3) and (8) results in good agreement for a number of materials over a wide porosity fraction range ($0.1 < P' < 0.7$) (ref. 21). In this case, the right-hand side of equation (8) is reduced such that:

$$V = V_o(1 - P') \qquad (9)$$

Equation (9) shows a linear relationship between velocity and porosity fraction and is the basis for selecting linear regression to analyze the empirical correlations reported in this study.

---

[1]Concerning the relationship between Poisson's ratio and porosity fraction, most of the limited studies of Poisson's ratio show it decreasing with increasing porosity fraction less rapidly than for elastic modulus (ref. 3). In this development, it is assumed that Poisson's ratio is independent of porosity fraction.

It is sometimes convenient to discuss the relationship between velocity and percent porosity, %P, where:

$$\%P = (P')100 \qquad (10)$$

Solving equation (10) for P' and substituting into equation (9) gives:

$$V = m(\%P) + V_o \qquad (11)$$

where

$$m = -V_o/100 \qquad (12)$$

Equation (11) shows a linear relationship between V and %P where m and V_o are the slope and intercept, respectively.

We can also define a "percent theoretical velocity," %TV, where:

$$\%TV = (V/V_o)100 \qquad (13)$$

Solving equation (13) for V and substituting into equation (11) gives:

$$\%TV = m'(\%P) + 100 \qquad (14)$$

where

$$m' = (m)100/V_o \qquad (15)$$

Equation (14) shows a linear relationship between %TV and %P where m' and 100 are the slope and intercept, respectively. Presenting the velocity versus porosity fraction relationship in terms of equation (14) is essentially a normalization procedure in that the theoretical velocity of a material and the type of wave (longitudinal or shear) used in the velocity measurement are "removed" as variables. From the derivative of equation (14), the following quantity can be defined:

$$(1/m') = (\Delta\%P/\Delta\%TV) \qquad (16)$$

where Δ is "change in."

DATA EXTRACTION PROCEDURE

Almost all of the data presented in this study were obtained from previously-published studies. The policy employed was that all of the available data should be tabulated and analyzed. In most cases, the reference provided V versus ρ data, either in the form of a table or plot. In some cases, the reference provided percent theoretical density ($\%\rho_o$) or P' values instead of ρ values. Where necessary, ρ and $\%\rho_o$ values were converted to %P values with the aid of equations (4) and (10).[2]

STATISTICAL ANALYSIS METHOD

Linear regression analysis and its associated statistics utilized in this study are briefly described in the next several paragraphs. The authors felt that a comprehensive set of statistics was necessary for this analysis because of the variation among data sets in the number of velocity measurements and the porosity fraction range over which those measurements were made.

Linear regression analysis is concerned with the problem of predicting or estimating the value of a (dependent) variable (V and %TV in equations (11) and (14), respectively) on the basis of another (independent) variable (%P in equations (11) and (14)). For the sake of simplicity, we have applied the classical regression model (ref. 23) which involves the following assumptions. V (and %TV) has been assumed to contain all the error while %P has been assumed to contain no

---

[2]In most cases, the references provided V and ρ data to 3 or 4 significant figures. For the sake of uniformity, all data and subsequent calculations including statistical values are presented in this report to at most 3 significant figures.

error.[3] The variance in V (and %TV) has been assumed to be constant for all values of %P, and the distribution about V has been assumed to be normal with mean values lying exactly on the regression line. It also has been assumed that only one V value was measured at a particular %P.

Linear regression analysis results in predicted slope (m and m' in eqs. (11) and (14), respectively) and intercept (V_o in eq. (11)) values that describe the relationship between V (and %TV) and %P. The Pearson product-moment correlation coefficient and level of significance statistics describe the quality of the regression. The correlation coefficient measures the strength of the linear relationship for the sample data. The level of significance, determined by the number of data points and the value of the correlation coefficient, determines an acceptance or confidence region for the regression. A level of significance of 0.025 corresponds to a 95 percent confidence region. The smaller (better) the level of significance, the lower the probability that the value of the correlation coefficient can be attributed to chance.

Confidence intervals for the predicted slope, intercept, and mean velocity values (the mean of further velocity measurements obtained at some %P value) are also presented. The 95 percent symmetric confidence interval was chosen for the analysis.[4] In practical terms, the 95 percent confidence interval means that in 95 percent of the cases, the true value of the parameter will fall within the calculated interval.

REVIEW AND ANALYSIS

The review and statistical analysis are presented in Table I and figures 1 to 61. Most of the figures show scatter plots of V versus %P data for Al_2O_3 (refs. 16, 24 to 27), CuO (ref. 28) MgO (ref. 29), porcelain-based ceramics (refs. 7, 30 and 31), PZT (ref. 8), SiC (refs. 26, 32 to 35), Si_3N_4 (refs. 36 to 38), steel (ref. 39), tungsten (ref. 2), UO_2 (ref. 40), $(U_{0.30}Pu_{0.70})C$ (ref. 41), and $YBa_2Cu_3O_{7-x}$ (refs. 11, 42 to 45). The table presents the linear regression statistics corresponding to the scatter plots. The 95 percent confidence interval for the predicted slope and intercept values are presented in table I while the 95 percent confidence interval for mean predicted velocity values is shown by

---

[3] An analysis assuming errors in both variables is significantly more complicated. For some data sets, the uncertainty in %P may in fact be comparable to that of V. The total uncertainties in each of %P and V including experimental uncertainties, uncertainties in extracting data from plots, and different assumed values of ρ_o are estimated to be less than 5 percent in all cases.

[4] The choice of a particular size confidence interval is "economic" rather than mathematical. It depends directly on the cost of an error, and hence on the frequency with which one can afford to be wrong. High confidence intervals lead to wide limits, and if these limits are too wide to be useful, the gap between them must be reduced either by accepting less confidence or by increasing the amount of data (ref. 23).

dashed lines on the scatter plots.[5] The quantity (Δ%P/Δ%TV) is provided for all plot lines in the corresponding table entries. (Note that this quantity also has a confidence interval associated with it, the width of which is similar to that for m').

Pertinent information concerning the reference's study including ultrasonic technique, measurement uncertainties,[6] microstructural anisotropy, material processing techniques, and velocity variation within specimens is also included in the table. A blank table entry indicates that the information was unavailable. The "comments" in the table give the number of data points for that particular reference and in some cases point out a major conclusion determined by the reference concerning the V versus %P data.

The figures are organized as follows. Figures 1 to 4, 6 to 9, 12 to 15, 17 to 23, 25, 26, 28, 29, 33 to 36, 38, 40 to 42, 44, 45, 48 to 50, 52 to 54, 57 to 59, show scatter plots of V (and %TV) versus %P for a single reference's data.[7] Results of multiple investigations for a specific material were also combined and analyzed as one data set in figures 5, 10, 37, 43, 46, 55, and 60. Additionally, plots comparing predicted (in most cases) regression lines obtained for a specific material from different investigations are given in figures 11, 16, 24, 27, 30 to 32, 39, 47, 51, 56, and 61. Where applicable for a material, scatter plots of longitudinal wave velocity data are presented before plots of shear wave velocity data. For most scatter plots, the solid line drawn is the linear regression line determined from the least-squares technique. For the plots with only two data points, a line is drawn through the points. In this case, the correlation coefficient, level of significance, and confidence interval statistics are not applicable.

---

[5]Several issues concerning the 95 percent confidence intervals for predicted intercept, slope, and mean velocity values need to be noted. First, the assumption of only one V value for a particular %P value is a conservative assumption that we know is false for some of the data sets in this review (see "comments" in table I). This assumption tends to make the limits of the confidence interval wider (worse) than if the confidence interval was calculated based on the mean of several velocity measurement values at a particular %P value. Second, the confidence intervals for predicted slope and intercept may not appear exactly symmetric in table I due to the round off procedure. Third, the 95 percent confidence interval for mean predicted velocity values is in most cases drawn (dashed line) over the entire %P range shown. In several cases, the interval extends beyond the %P range where velocity data exists. In these cases, the interval widens (worsens) as expected where no data exists.

[6]In most cases, the experimental uncertainties in the velocity and density measurements were provided by the reference. In the event that they were not, the uncertainties were estimated from the reference's description of samples and measurement techniques, and from our experience.

[7]Because the range of %P values for which velocity measurements were obtained varied from reference to reference, the ranges shown on the horizontal and vertical axes of the plots differ from one to the next, i.e., the plots are not standardized. In some cases, the plot axes had to be adjusted to allow the presentation of the 95 percent confidence interval for mean predicted velocity values.

DISCUSSION

General Observations

Correlation coefficients with magnitudes greater than 0.95 were obtained in 31 out of 42 cases. Levels of significance with magnitudes less than 0.025 were obtained in 36 out of 42 cases. For longitudinal wave velocity, predicted intercepts (V_o) ranged from 0.443 cm/μs for unpoled PZT4 and unpoled PZT5 of reference 8 to 1.23 cm/μs for SiC of reference 33. For shear wave velocity, predicted intercepts (V_o) ranged from 0.313 cm/μs for $YBa_2Cu_3O_{7-x}$ to 0.786 cm/μs for SiC of reference 26. The quantity ($\Delta\%P/\Delta\%TV$) ranged from -0.52 for porcelain of reference 7 and poled PZT4 of reference 8 to -8.26 for porcelain T2 of reference 31. It is understandable that these quantities vary from one material to the next since each material has different elastic properties and density (eq. (1)). Predicted intercepts (V_o) for a specific material from different investigations agree fairly well (see the plots and tabular entries for Al_2O_3, SiC, and Si_3N_4). Predicted slopes for a specific material from different investigations agree fairly well in most cases. However, significant slope disparity is evident for Al_2O_3; this may be due to the limited porosity range for the data of references 26 and 27 and the inclusion of green and prefired sample data in the cases of references 24 and 25. For reference 26, the limited porosity range over which data was obtained is manifested in extremely wide 95 percent confidence limits for predicted slope, intercept and mean velocity values. In fact, one of the bounds for the confidence limits for predicted slope is a positive value.

Table II compares V_o predicted from regression analysis with that calculated from equations (7) (longitudinal wave velocity) and (7a) (shear wave velocity) for several materials. Values of elastic modulus, Poisson's ratio, and density for fully-dense (single crystal and/or polycrystalline) materials used in the calculation are presented. The values of V_o predicted from regression and those obtained from calculation agree within approximately 17 percent in 16 out of 16 cases, and within approximately 6 percent in 11 out of 16 cases.

Other Microstructural Variables Affecting Velocity

Although porosity fraction seems to be a significant and perhaps the major microstructural feature affecting ultrasonic velocity, several references point to other microstructural variables having an impact on velocity. These include slight compositional variations (ref. 31), preferred domain orientation (ref. 8), particle contact anisotropy (ref. 39), pore size distribution and geometry (ref. 2), and type of agglomeration (ref. 25). These variables may result in differences in predicted intercept (V_o) and slope for what is believed to be the same material from different investigations. Thus, the authors feel that the most accurate and precise application of the ultrasonic velocity method for estimating porosity fraction first requires the development of accurate velocity versus porosity fraction relationships/calibrations for the specific material of interest.

Ramifications

The estimation of batch-to-batch, sample-to-sample and within-sample %P variations for a material can be accomplished if the quantity ($\Delta\%P/\Delta\%TV$) is known with reasonable confidence for that material. The nondestructive mapping of spatial porosity fraction variations within a sample by means of an ultrasonic scanning technique has been reported recently (refs. 50 and

51). This approach may also be useful in the analysis of the uniformity of composite materials (ref. 34).

CONCLUSION

A review and statistical analysis of the ultrasonic velocity method for estimating the porosity fraction in polycrystalline materials is presented. First, a semi-empirical model was developed showing the origin of the linear relationship between ultrasonic velocity and porosity fraction. Then, from a compilation of data produced by many researchers, scatter plots of velocity versus percent porosity data were shown for Al_2O_3, CuO, MgO, porcelain-based ceramics, PZT, SiC, Si_3N_4, steel, tungsten, UO_2, $(U_{0.30}Pu_{0.70})C$, and $YBa_2Cu_3O_{7-x}$. Linear regression analysis produced slope, intercept, correlation coefficient, level of significance, and confidence interval statistics for the data. Velocity values predicted from regression analysis for fully-dense materials are in good agreement with those calculated from elastic properties. The estimation of batch-to-batch, sample-to-sample, and within-sample variations in porosity fraction for a material can be accomplished with ultrasonic velocity measurements if reasonable confidence exists in the velocity versus percent porosity linear relationship.

REFERENCES

1. Goetzel, C.: Treatise on Powder Metallurgy. Wiley, 1963.

2. Smith, J.T.; and Lopilato, S.A.: The Correlation of Density of Porous Tungsten Billets and Ultrasonic-Wave Velocity. Trans. Metall. Soc. AIME, vol. 236, no. 4, Apr. 1966, pp. 597-598.

3. Rice, R.W.: Microstructure Dependence of Mechanical Behavior of Ceramics. Properties of Microstructure: Treatise on Materials Science and Technology, vol. 11, R.K. MacCrone, ed., Academic Press, 1977, pp. 199-381.

4. Knudsen, F.P.; Parker, H.S.; and Burdick, M.D.: Flexural Strength of Specimens Prepared from Several Uranium Dioxide Powders--Its Dependence on Porosity and Grain Size Anol the Influence of Additions of Titania. J. Am. Ceram. Soc., vol. 43, no. 12, Dec. 1960, pp. 641-647.

5. Burdick, M.D.; and Parker, H.S.: Effect of Particle Size Bulk Density and Strength Properties of Vranium Dioxide Specimens. J. Am. Ceram. Soc., vol. 39, no. 5, May 1956, pp. 181-187.

6. Williams, E.C.; Reid-Jones, R.C.; and Dorrill, D.T.: Trans. Brit. Ceram. Soc., vol. 62, 1963, pp. 405-420.

7. Boisson, J.; Platon, F.; and Boch, P.: Constanti Electriche E. Attrito Interno in Alconi Materiali in Funzione Della Porosita. Ceramurgia, anno VI, no. 2, 1976, pp. 74-76.

8. Patel, N.D.; and Nicholson, P.S.: Comparison of Piezoelectric Properties of Hot-Pressed and Sintered PZT. Am. Ceram. Soc. Bull., vol. 65, no. 5, May 1986, pp. 783-787.

9. Alford, N. McN.; et al.: The Effect of Density of Critical Current and Oxygen Stoichiometry of Y Ba_2Cuz $O_{(x)}$ Superconductors. Nature, vol. 332, Mar. 3, 1988, pp. 58-59.

10. Song, S.N.; et al.: High-Tc Superconductivity in Y-Ba-Cu-O System. Adv. Ceram. Mater., vol. 2, no. 3B, 1987, pp. 480-486.

11. Blendell, J.E.; et al.: Processing-Property Relations for YBz_2 Cu_3 $O_{(7-x)}$High-Tc Superconductors. Adv. Ceram. Mater., vol. 2, no. 3B, July 1987, pp. 512-529.

12. Jones, J.T.; and Berard, M.F.: Ceramics Industrial Processing and Testing, Iowa State University Press, 1972.

13. Vander Voort, G.F.: Metallography Principles and Practices. McGraw-Hill, 1984, p.426.

14. Clark, G.L.; and Liu, C.H.: Quanititave Determination of Porosity by X-Ray Absorption. Anal. Chem., vol. 29, no. 10, Oct. 1957, pp. 1539-1541.

15. Papadakis, E.P.: Absolute Accuracy of the Pulse-Echo Overlap Method and the Pulse Superposition Method for Ultrasonic Velocity. J. Acous. Soc. Am., vol. 52, no. 3, Pt. 2, Sept. 1972, pp. 843-846.

16. Nagarajan, A.: Ultrasonic Study of Elasticity-Porosity Relationship in Polycrystalline Alumina. J. Appl. Phys., vol. 42, no. 10, Sept. 1971, pp. 3693-3696.

17. Szilard, J.: Physical Principles of Ultrasonic Testing. Ultrasonic Testing, J. Szilard, ed., Wiley, 1982, pp. 1-23.

18. Ryshkewitch, E.: Compressive Strength of Porous Sintered Alumina and Zirconia to Ceramography. J. Am. Ceram. Soc., vol. 36, no. 2, Feb. 1953, pp. 65-68.

19. Spriggs, R.M.: Expression for Effect of Porosity on Elastic Modulus of Polycrystalline Refractory Materials, Particularly Aluminum Oxide. J. Am. Ceram. Soc., vol. 44, no. 12, Dec. 1961, pp. 628-629.

20. Soroka, I.; and Sereda, P.J.: Interrelation of Hardness Modulus of Elasticity and Porosity in Various Gypsum Systems. J. Am. Ceram. Soc., vol. 51, no. 6, June 1968, pp. 337-338.

21. Phani, K.K.; and Niyogi, S.K.: Porosity Dependence of Ultrasonic Velocity and Elastic Modulus in Sintered Uranium Dioxide--A Discussion. J. Mater. Sci. Lett., vol. 5, Apr. 1986, pp. 427-430.

22. Swokowski, E.W.: Calculus With Analytical Geometry. Prindle, Weber & Schmidt, 1975, p. 461.

23. Acton, F.S.: Analysis of Straight Line Data. Wiley, 1959.

24. Claytor, T.N.; et al.: Nondestructive Measurement of Microstructure Evolution in Ceramics. Mater. Eval., vol. 47, no. 5, May 1989, pp. 532-535.

25. Jones, M.P.; Blessing, G.V.; and Robbins, C.R.: Dry-Coupled Ultrasonic Elasticity Measurements of Sintered Ceramics. Mater. Eval., vol. 44, no. 1, June 1986, pp. 859-862.

26. Stang, D.S.: Unpublished research, NASA Lewis Research Center, Cleveland, Ohio.

27. Arons, R.M.; and Kupperman, D.S.: Use of Sound-Velocity Measurements to Evaluate the Effect of Hot Isostatic Pressing on the Porosity of Ceramic Solids. Mater. Eval., vol. 40, no. 10, Sept. 1982, pp. 1076-1078.

28. Roth, D.J.; and Dolhert, L.E.: Unpublished research, NASA Lewis Research Center, Cleveland, Ohio, 1990.

29. D.S. Kupperman; and H.B. Karplus: Ultrasonic Wave Propagation Characteristics of Green Ceramics. Am. Ceram. Soc. Bull., vol. 63, no. 12, Dec. (1984), pp. 1505-1509.

30. Prof. Dr. inż. Leszek Filipczynski; Dr. inż Zozislaw Pawlowski; and Dr. inż Jerry Wehr, Ultrasonic Methods of Testing Materials. 2nd Edition, Translation, Butterworths, 1966, p. 255.

31. Shyuller, K.G.; Khennike, G.V.; and Kovziridze, Z.D.: Specific Features of Structure Evaluation in a Low-Temperature Ceramics. Glass Ceramics, vol. 44, 1988, pp. 473-475.

32. Friedman, W.D.; et al.: Characterization of Green Ceramics With X-Ray Tomography and Ultrasonics. Nondestructive Testing: High Performance Ceramics; Proceedings. American Ceramic Society, 1987, pp. 128-131.

33. Baaklini, G.Y.; et al.: High Frequency Ultrasonic Characterization of Sintered Silicon Carbide. Am. Ceram. Soc., vol. 72, no. 3, March 1989, pp. 383-387.

34. Gruber, J.J.; Smith, J.M.; and Brockelman, R.H.: Ultrasonic Velocity C-Scans for Ceramic and Composite Material Characterization. Mater. Eval., vol. 46, no. 1, Jan. 1988, pp. 90-96.

35. Klima, S.J.; et al.: Ultrasonic Velocity for Estimating Density of Structural Ceramics. NASA TM-82765, 1981.

36. Derkacs, T.; Matay, I.M.; Brentnall, W.D.: Nondestructive Evaluation of Ceramics. Contract Report No.: AD-A027357, TRW-ER-7798-F; TRW, Inc., May 1976.

37. McLean, A.F., et al.: Brittle Materials Design, High Temperature Gas Turbine, Interim Report Number 7, July 1, 1974 to December 31, 1974, AMMRC CTR 75-8, Apr. 1975, p. 97. NOTE: RESTRICTED MATERIAL

38. Thorp, J.S.; and Bushell, T.G.: Ultrasonic Examination of Reaction-Bonded Silicon-Nitride. J. Mater. Sci., vol. 20, no. 6, June 1985, pp. 2265-2274.

39. Papadakis, E.P.; and Petersen, B.W.: Ultrasonic Velocity as a Predictor of Density in Sintered Powder Metal Parts. Mater. Eval., vol. 37, no. 5, Apr. 1979, pp. 76-80.

40. Panakkal, J.P.; and Ghosh, J.K.: Ultrasonic Velocity in Sintered Uranium-Dioxide Pellets. J. Mater. Sci. Lett., vol. 3, no. 9, 1984, pp. 835-836.

41. Ghosh, J.K.; Panakkal, J.P.; and Roy, P.R.: Ultrasonic Velocity Measurement in The Characterisation of Nuclear Fuel Pellets. World Conference on Nondestructive Testing, Butterworths, 1985, pp. 1201-1205.

42. Gaiduk, A.L.; et al.: High-Frequency Acoustic Properties of Yttrium Ceramic. Sov. J. Low Temp. Phys., vol. 14, no. 7, July 1988, pp. 395-402.

43. Roth, D.J.; Dolhert, L.E.; and Kerwin, D.P.: Unpublished research, NASA Lewis Research Center, Cleveland, Ohio, 1990.

44. Ledbetter, H.M.; et al.: Elastic Constants and De BYe Temperature of Polycrystalline $YBa_2Cu_3O_{7-x}$. J. Mater. Res., vol. 2, no. 6, Nov/Dec. 1987, pp. 786-789.

45. Round, R.; and Bridge, B.: Elastic-Constants of the High-Temperature Ceramic Superconductor $YBa_2Cu_3O_{7-x}$. J. Mater. Sci. Lett., vol. 6, no. 12, Dec. 1987, pp. 1471-1472.

46. Alford, N.McN., et al.: Physical and Mechanical Properties of $YBa_2Cu_3O_{(7-Si)}$ Superconductors. Mater. Sci., vol. 23, no. 3, March 1988, pp. 761-768.

47. G.E. Deiter, Mechanical Metallurgy. Third ed., McGraw-Hill, 1986, p.50.

48. Engineering Property Data On Selected Ceramics. Vol.III, Single Oxides. Metals and Ceramics Information Center, Battelle's Columbus Laboratories, Columbus, OH, 1981, pp. 5.4.1-25.

49. Engineering Property Data On Selected Ceramics. Vol. II., Carbides. Metals and Ceramics Information Center, Battelle' Columbus Laboratories, Columbus, OH, 1979, pp. 5.2.3-10.

50. Generazio, E.R.; Roth, D.J.; and Baaklini, G.Y.: Acoustic Imaging of Subtle Porosity Variations in Ceramics. Mater. Eval., vol. 46, no. 9, Sept. 1988, pp. 1338-1343.

51. E.R. Generazio; D.J. Roth; and D.B. Stang: Ultrasonic Imaging of Porosity Variations Produced During Sintering. J. Am. Ceram. Soc., vol. 72, no.7, July 1989, pp. 1282-1289.

LIST OF SYMBOLS AND ABBREVIATIONS FOR TABLE I.

V = Velocity (cm/μsec)
SV = Shear wave velocity (cm/μsec)
LV = Longitudinal wave velocity (cm/μsec)
%TV = Percent theoretical velocity
%P = Percent porosity
Wt. = Weight
β_0 = Predicted value of intercept (Theoretical velocity)
β'_0 = Predicted value of intercept (Percent theoretical velocity)
β_1 = Predicted value of slope (Velocity/percent porosity)
β'_1 = Predicted value of slope (Percent theoretical velocity/percent porosity)
N/A = Not applicable
RBSN = Reaction-bonded silicon nitride
Δ = Change in

(A blank appearing in a table entry indicates that the author did not mention the subject or the information was otherwise unavailable.)

TABLE I.—ULTRASONIC VELOCITY VERSUS P

Material	Reference	Processing Notes/ Chemical Additives	Microstructural Anisotropy	Velocity Measurement Technique	Velocity Measurement Uncertainty (%)	Density Measurement Technique	Density Measurement Uncertainty (%)	Theoretical Density, ρ_o, Used to Calculate % Porosity (g/cc)	Predicted Line Equation ($V = \beta_1 \cdot \%P + \beta_0$)
Al_2O_3	24	1.5 mol % Sintering aids	Insignificant	Longitudinal waves, 10 MHz	≤ 0.1	Dry-wt. dimensional	≤ 1	3.98	LV = −0.018 • %P +
Al_2O_3	25	Sintering aid, Binder, Plasticizer, Water		Thru-transmission and pulse-echo overlap, Longitudinal waves, Dry and wet coupling, 5 MHz	≤ 0.8	Dry-wt. dimensional and liquid-immersion	≤ 2	3.98	LV = −0.019 • %P + 1
Al_2O_3	16	Starting powders of various mean particle size, Binder		Pulse-echo transit time, Longitudinal waves, 10 MHz	≤ 1	Dry-wt. dimensional	< 0.5	3.98	LV = −0.007 • %P + 1
Al_2O_3	26	Lubricants, Plasticizer, Water	Insignificant	Pulse-echo/cross-correlation, Longitudinal waves, 50 MHz	≤ 0.2	Liquid-immersion	≤ 2	3.98	LV = −0.004 • %P + 1
Al_2O_3	16, 24-26			Longitudinal waves				3.98	LV = −0.016 • %P + 1
Al_2O_3	27		Insignificant	Pulse-echo overlap, Shear waves, 5 MHz	≤ 1	Dry-wt. dimensional	≤ 1	3.98	SV = −0.003 • %P + 0.6
Al_2O_3	24	1.5 mol % Sintering aids	Insignificant	Shear waves, 5 MHz	≤ 0.2	Dry-wt. dimensional	≤ 1	3.98	SV = −0.012 • %P + 0.6
Al_2O_3	25	Sintering aid, Binder, Plasticizer, Water		Thru-transmission and pulse-echo overlap, Shear waves, Dry and wet coupling, 1-5 MHz	≤ 1.8	Dry-wt. dimensional and liquid-immersion	≤ 2	3.98	SV = −0.010 • %P + 0.6
Al_2O_3	16	Starting powders of of various mean particle size, Binder		Pulse-echo transit time, Shear waves, 10 MHz	≤ 1	Dry-wt. dimensional	< 0.5	3.98	SV = −0.004 • %P + 0.62
Al_2O_3	16, 24, 25, 27			Shear waves				3.98	SV = −0.009 • %P + 0.69
Al_2O_3	16, 24-27								
CuO	28	Starting powders different for each of 2 disks		Pulse-echo/cross-correlation, Longitudinal waves, Dry coupling, 5 MHz	≤ 0.4	Dry-wt. dimensional	≤ 1	6.40	LV = −0.006 • %P + 0.474
"Green" MgO	29	20 wt.% Binder		Pulse-echo overlap, Longitudinal waves, 2.25 MHz	≤ 0.5	Dry-wt. dimensional	≤ 1	2.70	LV = −0.014 • %P + 0.817

FOLDOUT FRAME /

ρ)	Predicted Line Equation ($\%TV = \beta'_1 \cdot \%P + \beta'_0$)	Correlation Coefficient / Level of Significance	95% Confidence Intervals for Predicted Intercept (β_0) and Slope (β_1)	95% Confidence Intervals for Predicted Intercept (β'_0) and Slope (β'_1)	$\frac{\Delta\% P}{\Delta\% TV}$	Largest Velocity Variation Across One Surface of Specimen (%)	Comments	Corresponding Figure Number
1.09	%TV = −1.65 • %P + 100	−0.999 / 0.0001	$1.07 \le \beta_0 \le 1.12$ $-0.019 \le \beta_1 \le -0.017$	$97.7 \le \beta'_0 \le 102$ $-1.77 \le \beta'_1 \le -1.52$	−0.61	15	5 data points lumped together in low % porosity region separated widely from 1 data point in high % porosity (Partially-fired specimen)	1
1.13	%TV = −1.64 • %P + 100	−0.992 / 0.0001	$0.994 \le \beta_0 \le 1.27$ $-0.022 \le \beta_1 \le -0.015$	$87.8 \le \beta'_0 \le 112$ $-1.94 \le \beta'_1 \le -1.34$	−0.61	1	Velocity may be very slightly sensitive to the type of agglomerates found in ceramic samples, which may depend on whether sample is calcined or not; 2 data points in low % porosity region widely separated from other 4 data points in high % porosity region (Green samples)	2
1.00	%TV = −0.736 • %P + 100	−0.928 / 0.0001	$0.987 \le \beta_0 \le 1.02$ $-0.008 \le \beta_1 \le -0.007$	$98.3 \le \beta'_0 \le 102$ $-0.818 \le \beta'_1 \le -0.654$	−1.36		16 data points	3
1.01	%TV = −0.377 • %P + 100	−0.698 / 0.302	$0.923 \le \beta_0 \le 1.09$ $-0.016 \le \beta_1 \le 0.008$	$92.2 \le \beta'_0 \le 108$ $-1.54 \le \beta'_1 \le 0.782$	−2.65	1	Limited data region; 4 data points	4
1.10	%TV = −1.43 • %P + 100	−0.949 / 0.0001	$1.06 \le \beta_0 \le 1.15$ $-0.018 \le \beta_1 \le -0.013$	$95.7 \le \beta'_0 \le 104$ $-1.61 \le \beta'_1 \le -1.25$	−0.699		32 data points, all longitudinal wave data	5
) 669	%TV = −0.477 • %P + 100	−0.94 / 0.006	$0.646 \le \beta_0 \le 0.692$ $-0.005 \le \beta_1 \le -0.002$	$96.7 \le \beta'_0 \le 103$ $-0.669 \le \beta'_1 \le -0.284$	−2.10	2	6 data points	6
) 655	%TV = −1.87 • %P + 100	−1.0 / 0.0001	$0.648 \le \beta_0 \le 0.663$ $-0.013 \le \beta_1 \le -0.012$	$98.9 \le \beta'_0 \le 101$ $-1.93 \le \beta'_1 \le -1.81$	−0.53	15	5 data points lumped together in low % porosity region separated widely from 1 data point in high % porosity region (Partially-fired specimen)	7
) 666	%TV = −1.55 • %P + 100	−0.987 / 0.0003	$0.571 \le \beta_0 \le 0.762$ $-0.008 \le \beta_1 \le -0.013$	$85.7 \le \beta'_0 \le 114$ $-1.90 \le \beta'_1 \le -1.20$	−0.65	1	Velocity may be very slightly sensitive to the type of agglomerates found in ceramic samples, which may depend on whether sample is calcined or not; 2 data points in low % porosity region widely separated from other 4 data points in high % porosity region (Green samples)	8
628	%TV = −0.662 • %P + 100	−0.990 / 0.0001	$0.622 \le \beta_0 \le 0.635$ $-0.005 \le \beta_1 \le -0.004$	$99.0 \le \beta'_0 \le 101$ $-0.705 \le \beta'_1 \le -0.610$	−1.51		17 data points	9
693	%TV = −1.35 • %P + 100	−0.910 / 0.0001	$0.656 \le \beta_0 \le 0.729$ $-0.011 \le \beta_1 \le -0.008$	$94.8 \le \beta'_0 \le 105$ $-1.57 \le \beta'_1 \le -1.14$	−0.741		35 data points, all shear wave data	10
							Comparison	11
474	%TV = −1.34 • %P + 100	−0.990 / 0.0100	$0.400 \le \beta_0 \le 0.549$ $-0.009 \le \beta_1 \le -0.004$	$84.3 \le \beta'_0 \le 116$ $-1.92 \le \beta'_1 \le -0.760$	−0.746		4 data points, 4 specimens cut from 2 disks, CuO phase confirmed from x-ray diffraction	12
817	N/A	−1.0 / 0.012	$0.673 \le \beta_0 \le 0.961$ $-0.017 \le \beta_1 \le -0.010$	N/A	−0.60	2	3 data points; material is unsintered, green compact	13

FOLDOUT FRAME 2

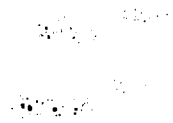

TABLE I.—ULTRASONIC VELOCITY VERSUS PERCENT POROSITY

Material	Reference	Processing Notes/ Chemical Additives	Microstructural Anisotropy	Velocity Measurement Technique	Velocity Measurement Uncertainty (%)	Density Measurement Technique	Density Measurement Uncertainty (%)	Theoretical Density, ρ_o, Used to Calculate % Porosity (g/cc)	Predicted Line Equation ($V = \beta_1 \cdot \%P + \beta_0$)	
Porcelain	7		Preferred granular orientation	Pulse-echo overlap, Longitudinal waves, 2 MHz	≤ 0.1	Dry-wt. dimensional	≤ 1	2.6	LV = −0.013 • %P + 0.728	%T
Porcelain	7		Preferred granular orientation	Pulse-echo overlap, Shear waves, 2 MHz	≤ 0.1	Dry-wt. dimensional	≤ 1	2.6	SV = −0.009 • %P + 0.448	%T
Porcelain	7									
Porcelain	30			Longitudinal waves, 1.5–3 MHz				2.60	LV = −0.006 • %P + 0.618	%TV
Porcelain P1 (See ref.)	31	(See ref.)		Longitudinal waves, 15 MHz	≤ 1	Dry-wt. dimensional	≤ 1	2.51	LV = −0.002 • %P + 0.611	%TV
Porcelain P2 (See ref.)	31	(See ref.)		Longitudinal waves, 15 MHz	≤ 1	Dry-wt. dimensional	≤ 1	2.56	LV = −0.005 • %P + 0.615	%TV
Porcelain T1 (See ref.)	31	(See ref.)		Longitudinal waves, 15 MHz	≤ 1	Dry-wt. dimensional	≤ 1	2.58	LV = −0.001 • %P + 0.623	%TV
Porcelain T2 (See ref.)	31	(See ref.)		Longitudinal waves, 15 MHz	≤ 1	Dry-wt. dimensional	≤ 1	2.64	LV = −0.0008 • %P + 0.626	%TV
Unpoled PZT4	8		Insignificant	Pulse-echo overlap, Longitudinal waves, 50 MHz	≤ 0.1	Liquid-immersion	≤ 2	8.0	LV = −0.007 • %P + 0.443	%TV
Poled PZT4	8		Preferred electrical domain orientation	Pulse-echo overlap, Longitudinal waves, 50 MHz	≤ 0.1	Liquid-immersion	≤ 2	8.0	LV = −0.009 • %P + 0.483	%TV
PZT4	8									
Unpoled PZT5	8		Insignificant	Pulse-echo overlap, Longitudinal waves, 50 MHz	≤ 0.1	Liquid-immersion	≤ 2	8.0	LV = −0.008 • %P + 0.443	%TV =
Poled PZT5	8		Preferred electrical domain orientation	Pulse-echo overlap, Longitudinal waves, 50 MHz	≤ 0.1	Liquid-immersion	≤ 2	8.0	LV = −0.010 • %P + 0.486	%TV =
PZT5	8									

FOLDOUT FRAME 1

POROSITY: REVIEW AND STATISTICAL ANALYSIS—CONTINUED

	Predicted Line Equation ($\%TV = \beta'_1 \cdot \%P + \beta'_0$)	Correlation Coefficient / Level of Significance	95% Confidence Intervals for Predicted Intercept (β_0) and Slope (β_1)	95% Confidence Intervals for Predicted Intercept (β'_0) and Slope (β'_1)	$\frac{\Delta\% P}{\Delta\% TV}$	Largest Velocity Variation Across One Surface of Specimen (%)	Comments	Corresponding Figure Number
728	%TV = −1.78 • %P + 100	−0.993 / 0.0001	$0.713 \le \beta_0 \le 0.743$ $-0.0014 \le \beta_1 \le -0.0012$	$97.9 \le \beta'_0 \le 102$ $-1.87 \le \beta'_1 \le -1.70$	−0.56		27 data points; multiphase ceramic; sample composition and thus theoretical density vary slightly with firing temperature; measurements made along extrusion axis	14
448	%TV = −1.93 • %P + 100	−0.998 / 0.0001	$0.442 \le \beta_0 \le 0.454$ $-0.009 \le \beta_1 \le -0.008$	$98.7 \le \beta'_0 \le 101$ $-1.98 \le \beta'_1 \le -1.88$	−0.52			15
							Comparison	16
618	%TV = −0.935 • %P + 100	−0.987 / 0.0001	$0.606 \le \beta_0 \le 0.630$ $-0.007 \le \beta_1 \le -0.005$	$98.1 \le \beta'_0 \le 102$ $-1.11 \le \beta'_1 \le -0.760$	−1.07		7 data points; multiphase ceramic; sample composition and thus theoretical density vary slightly with firing temp	17
611	%TV = −0.312 • %P + 100	−0.586 / 0.414	$0.553 \le \beta_0 \le 0.668$ $-0.010 \le \beta_1 \le 0.006$	$90.5 \le \beta'_0 \le 109$ $-1.34 \le \beta'_1 \le -1.28$	−3.21		4 data points; multiphase ceramic; sample composition and thus theoretical density vary slightly with firing temp.	18
615	%TV = −0.740 • %P + 100	−0.983 / 0.017	$0.598 \le \beta_0 \le 0.631$ $-0.007 \le \beta_1 \le -0.002$	$97.3 \le \beta'_0 \le 102$ $-1.04 \le \beta'_1 \le -0.436$	−1.35			19
623	%TV = −0.167 • P + 100	−0.894 / 0.106	$0.612 \le \beta_0 \le 0.632$ $-0.003 \le \beta_1 \le 0.0005$	$98.6 \le \beta'_0 \le 101$ $-0.422 \le \beta'_1 \le 0.088$	−5.99			20
626	%TV = −0.121 • %P + 100	−0.947 / 0.053	$0.621 \le \beta_0 \le 0.631$ $-0.002 \le \beta_1 \le 0.003$	$99.2 \le \beta'_0 \le 101$ $-0.246 \le \beta'_1 \le 0.004$	−8.26			21
443	%TV = −1.68 • %P + 100	N/A / N/A	N/A	N/A	−0.60		2 data points for each set; PZT4, PZT5, and PZT7 are each different solid solution combinations of $PbZrO_3$ and $PbTiO_3$ but theoretical density is ~8.0 g/cc for each; poling orients electric domains; velocity measured along polarized direction for poled specimens; no correlation coefficient is given since only 2 data points for each set; all poled sets have higher theoretical velocity than corresponding unpoled set	22
483	%TV = −1.93 • %P + 100	N/A / N/A	N/A	N/A	−0.52			23
							Comparison	24
443	%TV = −1.85 • %P + 100	N/A / N/A	N/A	N/A	−0.54		2 data points for each set; PZT4, PZT5, and PZT7 are each different solid solution combinations of $PbZrO_3$ and $PbTiO_3$ but theoretical density is ~8.0 g/cc for each; poling orients electric domains; velocity measured along polarized direction for poled specimens; no correlation coefficient is given since only 2 data points for each set; all poled sets have higher theoretical velocity than corresponding unpoled set	25
486	%TV = −2.12 • %P + 100	N/A / N/A	N/A	N/A	−0.47			26
							Comparison	27

FOLDOUT FRAME 2

TABLE I.—ULTRASONIC VELOCITY VERSUS PERC

Material	Reference	Processing Notes/ Chemical Additives	Microstructural Anisotropy	Velocity Measurement Technique	Velocity Measurement Uncertainty (%)	Density Measurement Technique	Density Measurement Uncertainty (%)	Theoretical Density, ρ_o, Used to Calculate % Porosity (g/cc)	Predicted Line Equation ($V = \beta_1 \cdot \%P +$
Unpoled PZT7	8		Insignificant	Pulse-echo overlap, Longitudinal waves, 50 MHz	≤ 0.1	Liquid-immersion	≤ 2	8.0	LV = −0.004 • %P +
Poled PZT7	8		Preferred electrical domain orientation	Pulse-echo overlap, Longitudinal waves, 50 MHz	≤ 0.1	Liquid-immersion	≤ 2	8.0	LV = −0.005 • %P +
PZT7	8								
Unpoled PZT	8								
Poled PZT	8								
"Green" α-SiC	32	Binder		Thru-transmission transit time, Longitudinal waves, 500 KHz	≤ 1	Liquid-immersion	≤ 2	3.22	LV = −0.007 • %P +
α-SiC	33	Boron and carbonaceous resin binders	Some specimens have preferred pore orientation	Pulse-echo/cross-correlation, Longitudinal waves, 100 MHz	≤ 0.1	Dry-wt. dimensional	≤ 1	3.22	LV = −0.014 • %P +
α-SiC	34			Pulse-echo overlap, Longitudinal waves, 25 MHz	≤ 1	Liquid-immersion	≤ 2	3.22	LV = −0.011 • %P + 1
α-SiC	35		Insignificant	Pulse-echo overlap, Longitudinal waves, 20 MHz	≤ 1	Dry-wt. dimensional	≤ 1	3.22	LV = −0.011 • %P + 1.2
α-SiC	33-35			Longitudinal waves				3.22	LV = −0.011 • %P + 1.2
α-SiC	26	Boron and carbonaceous resin binders	Some specimens have preferred pore orientation	Pulse-echo/cross-correlation, Shear waves, 20 MHz	≤ 0.1	Liquid-immersion	≤ 2	3.22	SV = −0.009 • %P + 0.78
α-SiC	26, 33-35								
Si_3N_4	36	Hot-pressed silicon nitride has 1% MgO sintering aid and 0.5-1% impurities, RBSN has < 1% impurities and various amounts of unreacted silicon	Insignificant	Pulse-echo overlap, Longitudinal waves, 25-45 MHz	≤ 1	Dry-wt. dimensional	≤ 1	3.30	LV = −0.015 • %P + 1.11

FOLDOUT FRAME 1

)	Predicted Line Equation (%TV = β'_1 • %P + β'_0)	Correlation Coefficient / Level of Significance	95% Confidence Intervals for Predicted Intercept (β_0) and Slope (β_1)	95% Confidence Intervals for Predicted Intercept (β'_0) and Slope (β'_1)	$\frac{\Delta\%\ P}{\Delta\%\ TV}$	Largest Velocity Variation Across One Surface of Specimen (%)	Comments	Corresponding Figure Number
) 464	%TV = −0.760 • %P + 100	N/A / N/A	N/A	N/A	−1.32		2 data points for each set, PZT4, PZT5, and PZT7 are each different solid solution combinations of $PbZrO_3$ and $Pb\ TiO_3$ but theoretical density is ~8.0 g/cc for each; poling orients electric domains; velocity measured along polarized direction for poled specimens; no correlation coefficient is given since only 2 data points for each set; all poled sets have higher theoretical velocity than corresponding unpoled set	28
) 494	%TV = −0.952 • %P + 100	N/A / N/A	N/A	N/A	−1.05			29
							Comparison	30
							Comparison	31
							Comparison	32
) 464	N/A	−0.974 / 0.0001	$0.397 \le \beta_0 \le 0.535$ $-0.009 \le \beta_1 \le -0.006$	N/A	−0.633	30	8 data points; material is unsintered green compact; large velocity variation even though small density variation within specimen; quality of contact between individual powder particles may affect velocity	33
23	%TV = −1.16 • %P + 100	−0.993 / 0.0001	$1.22 \le \beta_0 \le 1.24$ $-0.016 \le \beta_1 \le -0.013$	$99.4 \le \beta'_0 \le 101$ $-1.29 \le \beta'_1 \le -1.03$	−0.862	≤ 0.1	8 data points; each data point is for a particular batch and is the average of ~24 measurements on ~8 specimens. Velocity not greatly sensitive to mean pore size, mean pore orientation, and mean grain size	34
21	%TV = −0.916 • %P + 100	−0.999 / 0.0001	$1.21 \le \beta_0 \le 1.22$ $-0.012 \le \beta_1 \le -0.011$	$99.8 \le \beta'_0 \le 100$ $-0.962 \le \beta'_1 \le -0.870$	−1.09	< 5	6 data points	35
22	%TV = −0.883 • %P + 100	−0.957 / 0.0001	$1.22 \le \beta_0 \le 1.22$ $-0.011 \le \beta_1 \le -0.010$	$99.9 \le \beta'_0 \le 100$ $-0.939 \le \beta'_1 \le 0.832$	−1.13	< 1	194 data points	36
22	%TV = −0.912 • %P + 100	−0.964 / 0.0001	$1.216 \le \beta_0 \le 1.220$ $-0.012 \le \beta_1 \le -0.011$	$99.9 \le \beta'_0 \le 100$ $-0.939 \le \beta'_1 \le -0.832$	−1.10		208 data points, all longitudinal wave data	37
786	%TV = −1.16 • %P + 100	−0.991 / 0.0001	$0.711 \le \beta_0 \le 0.859$ $-0.010 \le \beta_1 \le -0.008$	$99.0 \le \beta'_0 \le 101$ $-1.32 \le \beta'_1 \le -1.01$	−0.86	≤ 0.1	8 data points, most specimens from same batches used by Baaklini	38
							Comparison	39
11	%TV = −1.34 • %P + 100	N/A / N/A	N/A	N/A	−0.75		No correlation coefficient is given since only 2 data points, but each point is average of measurement on 25 specimens, data point in low % porosity region is for hot-pressed Si_3N_4 while data point in high % porosity is for reaction-bonded Si_3N_4	40

FOLDOUT FRAME 2

TABLE I.—ULTRASONIC VELOCITY VERSUS PERCENT

Material	Reference	Processing Notes/ Chemical Additives	Microstructural Anisotropy	Velocity Measurement Technique	Velocity Measurement Uncertainty (%)	Density Measurement Technique	Density Measurement Uncertainty (%)	Theoretical Density, ρ_0, Used to Calculate % Porosity (g/cc)	Predicted Line Equation ($V = \beta_1 \cdot \%P + \beta_0$)
Si_3N_4	37	Injection-molded, slip-cast, and hot-pressed specimens		Thru-transmission transit time, Longitudinal waves, 5 MHz				3.30	LV = −0.016 • %P + 1
Si_3N_4	38	RBSN has < 1% impurities and various amounts of unreacted silicon	Insignificant	Pulse-echo overlap, Longitudinal waves, 15 MHz	≤ 0.1	Dry-wt dimensional	≤ 0.1	3.30	LV = −0.013 • %P + 1
Si_3N_4	36-38			Longitudinal waves				3.30	LV = −0.014 • %P + 1
Si_3N_4	37	Injection-molded, slip-cast, and hot-pressed specimens		Thru-transmission transit time, Shear waves, 5 MHz				3.30	SV = −0.008 • %P + 0.6
Si_3N_4	38	RBSN has < 1% impurities and various amounts of unreacted silicon	Insignificant	Pulse-echo overlap, Shear waves, 15 MHz	≤ 0.1	Dry-wt dimensional	≤ 0.1	3.30	SV = −0.007 • %P + 0.6
Si_3N_4	37, 38			Shear waves				3.30	SV = −0.007 • %P + 0.64
Si_3N_4	36-38								
Steel A-direction (See ref.)	39		Possibly particle contact anistropy (≤ 5%) based on pressing direction	Thru-transmission pulse-echo overlap, Dry coupling, Longitudinal waves, 1.5–2.25 MHz	≤ 0.01	ASTM B-328-60	Undetermined, probably ≤ 2%	7.85	LV = −0.007 • %P + 0.56
Steel B-direction (See ref.)	39			Thru-transmission pulse-echo overlap, Dry coupling, Longitudinal waves, 1.5–2.25 MHz	≤ 0.01	ASTM B-328-60	Undetermined, probably ≤ 2%	7.85	LV = −0.009 • %P + 0.58
Steel C-direction (See ref.)	39			Thru-transmission pulse-echo overlap, Dry coupling, Longitudinal waves, 1.5–2.25 MHz	≤ 0.01	ASTM B-328-60	Undetermined, probably ≤ 2%	7.85	LV = −0.009 • %P + 0.59
Steel	39								

FOLDOUT FRAME 1

)	Predicted Line Equation (%TV = β'_1 • %P + β'_0)	Correlation Coefficient / Level of Significance	95% Confidence Intervals for Predicted Intercept (β_0) and Slope (β_1)	95% Confidence Intervals for Predicted Intercept (β'_0) and Slope (β'_1)	$\frac{\Delta\%\ P}{\Delta\%\ TV}$	Largest Velocity Variation Across One Surface of Specimen (%)	Comments	Corresponding Figure Number
1.14	%TV = −1.41 • %P + 100	−0.997 / 0.0001	$1.12 \le \beta_0 \le 1.16$ $-0.017 \le \beta_1 \le -0.015$	$98.6 \le \beta'_0 \le 101$ $-1.48 \le \beta'_1 \le -1.34$	−0.71		13 data points	41
1.12	%TV = −1.15 • %P + 100	−0.991 / 0.001	$0.928 \le \beta_0 \le 1.25$ $-0.016 \le \beta_1 \le -0.010$	$88.0 \le \beta'_0 \le 111$ $-1.44 \le \beta'_1 \le -0.864$	−0.87		5 data points	42
1.12	%TV = −1.27 • %P + 100	−0.981 / 0.0001	$1.08 \le \beta_0 \le 1.15$ $-0.016 \le \beta_1 \le -0.013$	$97.1 \le \beta'_0 \le 103$ $-1.40 \le \beta'_1 \le -1.15$	−0.787		20 data points, all longitudinal wave data	43
1.652	%TV = −1.18 • %P + 100	−0.991 / 0.0001	$0.636 \le \beta_0 \le 0.667$ $-0.008 \le \beta_1 \le 0.007$	$97.6 \le \beta'_0 \le 102$ $-1.30 \le \beta'_1 \le -1.06$	−0.85		11 data points	44
1.675	%TV = −1.10 • %P + 100	−0.984 / 0.002	$0.574 \le \beta_0 \le 0.776$ $-0.011 \le \beta_1 \le -0.004$	$85.0 \le \beta'_0 \le 115$ $-1.62 \le \beta'_1 \le -0.580$	−0.91		5 data points	45
645	%TV = −1.07 • %P + 100	−0.973 / 0.0001	$0.624 \le \beta_0 \le 0.666$ $-0.008 \le \beta_1 \le -0.006$	$96.6 \le \beta'_0 \le 103$ $-1.22 \le \beta'_1 \le -0.928$	−0.935		16 data points, all shear wave data	46
							Comparison	47
563	%TV = −1.19 • %P + 100	−0.972 / 0.0001	$0.551 \le \beta_0 \le 0.574$ $-0.007 \le \beta_1 \le -0.006$	$98.0 \le \beta'_0 \le 102$ $-1.32 \le \beta'_1 \le -1.06$	−0.84		Measurements made in 3 directions (A, B, C) with respect to pressing direction for sintered steel rectangles, some residual particle contact anistropy may be responsible for small directional dependence of velocity, velocity also may be path-length dependent 22 data points for A-direction 16 data points for B-direction 18 data points for C-direction	48
588	%TV = −1.53 • %P + 100	−0.985 / 0.0001	$0.573 \le \beta_0 \le 0.602$ $-0.010 \le \beta_1 \le -0.008$	$97.6 \le \beta'_0 \le 102$ $1.68 \le \beta'_1 \le -1.37$	−0.65			49
590	%TV = −1.48 • %P + 100	−0.996 / 0.0001	$0.583 \le \beta_0 \le 0.597$ $-0.009 \le \beta_1 \le -0.008$	$98.8 \le \beta'_0 \le 101$ $-1.54 \le \beta'_1 \le -1.41$	−0.68			50
							Comparison	51

FOLDOUT FRAME 2

TABLE I.—ULTRASONIC VELOCITY VERSUS PERCENT POROSITY: RE

Material	Reference	Processing Notes/ Chemical Additives	Microstructural Anisotropy	Velocity Measurement Technique	Velocity Measurement Uncertainty (%)	Density Measurement Technique	Density Measurement Uncertainty (%)	Theoretical Density, ρ_0, Used to Calculate % Porosity (g/cc)	Predicted Line Equation ($V = \beta_1 \cdot \%P + \beta_0$)	Predi (%TV
Tungsten	2	Kenna nominal 4 micron starting powder size		Thru-transmission pulse-echo overlap, Longitudinal waves, 1 MHz	≤ 0.5	ASTM C20-46 Liquid-immersion	≤ 2	19.3	LV = −0.005 • %P + 0.520	%TV =
Tungsten	2	G.E. nominal 4 micron starting powder size		Thru-transmission pulse-echo overlap, Longitudinal waves, 1 MHz	≤ 0.5	ASTM C20-46 Liquid-immersion	≤ 2	19.3	LV = −0.006 • %P + 0.558	%TV =
Tungsten	2	G.E. nominal 18 micron starting powder size		Thru-transmission pulse-echo overlap, Longitudinal waves, 1 MHz	≤ 0.5	ASTM C20-46 Liquid-immersion	≤ 2	19.3	LV = −0.008 • %P + 0.554	%TV =
Tungsten	2			Longitudinal waves				19.3	LV = −0.006 • %P + 0.533	%TV =
Tungsten	2									
UO_2	40			Thickness-cum-velocity meter, Longitudinal waves, 10 MHz	≤ 1	ASTM C-753-88	≤ 2	10.96	LV = −0.008 • %P + 0.550	%TV =
$(U_{0.30}Pu_{0.70})C$	41			Thickness-cum-velocity meter, Longitudinal waves, 15 MHz	≤ 1	ASTM C-753-88	≤ 2	12.19	LV = −0.004 • %P + 0.460	%TV = −
$YBa_2Cu_3O_{7-x}$	43	Different starting powders		Pulse-echo/cross-correlation, Longitudinal waves, Dry and wet coupling, 5-20 MHz	≤ 0.4	Dry-wt dimensional	≤ 1	6.38	LV = −0.007 • %P + 0.565	%TV = −

FOLDOUT FRAME /

POROSITY: REVIEW AND STATISTICAL ANALYSIS—CONTINUED

	Predicted Line Equation ($\%TV = \beta'_1 \cdot \%P + \beta'_0$)	Correlation Coefficient / Level of Significance	95% Confidence Intervals for Predicted Intercept (β_0) and Slope (β_1)	95% Confidence Intervals for Predicted Intercept (β'_0) and Slope (β'_1)	$\frac{\Delta\% P}{\Delta\% TV}$	Largest Velocity Variation Across One Surface of Specimen (%)	Comments	Corresponding Figure Number
520	%TV = −0.939 • %P + 100	−0.960 / 0.010	$0.465 \le \beta_0 \le 0.575$ $-0.007 \le \beta_1 \le -0.003$	$89.4 \le \beta'_0 \le 111$ $-1.38 \le \beta'_1 \le -0.501$	−1.06		Velocity shown to be sensitive to pore size distribution/mean pore size and grain size distribution/mean grain size which is a function of starting powder size distribution. These results show different theoretical velocity for tungsten depending on the starting powder size. 5 data points for Kenna 4 μm powder, 5 data points for GE 4 μm powder, 4 data points for GE 18 μm powder Each data point is average of 17 measurements across sample	52
558	%TV = −1.13 • %P + 100	−0.918 / 0.028	$0.387 \le \beta_0 \le 0.729$ $-0.007 \le \beta_1 \le -0.006$	$69.3 \le \beta'_0 \le 131$ $-1.92 \le \beta'_1 \le -0.351$	−0.88			53
554	%TV = −1.38 • %P + 100	−0.992 / 0.008	$0.471 \le \beta_0 \le 0.637$ $-0.011 \le \beta_1 \le -0.005$	$85.1 \le \beta'_0 \le 115$ $-1.92 \le \beta'_1 \le -0.832$	−0.72			54
533	%TV = −1.11 • %P + 100	−0.916 / 0.0001	$0.482 \le \beta_0 \le 0.583$ $-0.008 \le \beta_1 \le -0.004$	$90.5 \le \beta'_0 \le 109$ $-1.41 \le \beta'_1 \le -0.802$	−0.901		14 data points, all longitudinal wave data	55
							Comparison	56
550	%TV = −1.49 • %P + 100	−0.997 / 0.0001	$0.547 \le \beta_0 \le 0.552$ $-0.009 \le \beta_1 \le 0.008$	$99.5 \le \beta'_0 \le 100$ $-2.09 \le \beta'_1 \le -0.883$	−0.67		17 data points	57
460	%TV = −0.958 • %P + 100	−0.949 / 0.051	$0.422 \le \beta_0 \le 0.496$ $-0.009 \le \beta_1 \le 0.00003$	$92.0 \le \beta'_0 \le 108$ $-1.92 \le \beta'_1 \le 0.005$	−1.04		4 data points	58
465	%TV = −1.28 • %P + 100	−0.991 / 0.0001	$0.554 < \beta_0 < 0.576$ $-0.008 < \beta_1 < -0.007$	$98.0 < \beta'_0 < 102$ $-1.39 < \beta'_1 < -1.16$	−0.781		13 data points	59

FOLDOUT FRAME 2

TABLE I.—ULTRASONIC VELOCITY VERSUS PERCENT P

Material	Reference	Processing Notes/ Chemical Additives	Microstructural Anisotropy	Velocity Measurement Technique	Velocity Measurement Uncertainty (%)	Density Measurement Technique	Density Measurement Uncertainty (%)	Theoretical Density, ρ_0, Used to Calculate % Porosity (g/cc)	Predicted Line Equation ($V = \beta_1 \cdot \%P + \beta_0$)
$YBa_2Cu_3O_{7-x}$ Superconductor	43		Insignificant	Pulse-echo/cross-correlation, Shear waves, 10 MHz	≤ 0.4	Dry-wt dimensional	≤ 1	6.38	SV = −0.002 • %P + 0.31
	42			Phase comparison method, Shear waves, 50 MHz	≤ 2				
	11			Pulse-echo overlap, Shear waves, 3-10 MHz	≤ 1 dimensional	Dry-wt	≤ 1		
	44			Pulse-echo matchup, Shear waves, 3-4 MHz	≤ 1	Dry-wt dimensional	≤ 1		
	45			Thru-transmission pulse-echo overlap, Shear waves, 5 MHz	≤ 3	Liquid-immersion	≤ 2		
$YBa_2Cu_3O_{7-x}$	11, 42-45								

FOLDOUT FRAME 1

POROSITY: REVIEW AND STATISTICAL ANALYSIS—CONCLUDED

	Predicted Line Equation ($\%TV = \beta'_1 \cdot \%P + \beta'_0$)	Correlation Coefficient / Level of Significance	95% Confidence Intervals for Predicted Intercept (β_0) and Slope (β_1)	95% Confidence Intervals for Predicted Intercept (β'_0) and Slope (β'_1)	$\frac{\Delta\% P}{\Delta\% TV}$	Largest Velocity Variation Across One Surface of Specimen (%)	Comments	Corresponding Figure Number
							1 data point; sample was single-phase, untextured, and free of nonuniform stress	
							1 data point	
13	$\%TV = -0.768 \cdot \%P + 100$	$\frac{-0.814}{0.0486}$	$0.252 \le \beta_0 \le 0.373$ $-0.005 \le \beta_1 \le -0.00002$	$81.6 \le \beta'_0 \le 119$ $-1.53 \le \beta'_1 \le -0.007$	-1.30		2 data points, samples are not compositionally homogeneous	60
							1 data point	
							1 data point	
							Comparison	61

FOLDOUT FRAME 2

TABLE II.—COMPARISON OF V_o PREDICTED FROM REGRESSION ANALYSIS WITH THAT CALCULATED FROM EQUATIONS 7 (LONGITUDINAL VELOCITY) AND 7a (SHEAR WAVE VELOCITY)

		Longitudinal Wave Velocity			Shear Wave Velocity			Values substituted into eqs. (7) [For Longitudinal Wave Velocity] and (7a) [For Shear Wave Velocity] to obtain V_{oC}		
Material	Single crystal (S) or poly-crystalline (P)	Average V_o from regression (V_{oR}) [cm/μsec]	Calculated V_o from eq. (7) (V_{oC}) [cm/μsec]	% Variation between V_{oC} and V_{oR} = $100 \lvert V_{oC} - V_{oR} \rvert / V_{oC}$	Average V_o from regression (V_{oR}) [cm/μsec]	Calculated V_o from eq. (7a) (V_{oC}) [cm/μsec]	% Variation between V_{oC} and V_{oR} = $100 \lvert V_{oC} - V_{oR} \rvert / V_{oC}$	Fully-dense elastic modulus, E_o (x 10-6) psi /(ref.)	Poisson's ratio, ν/(ref.)	Theoretical density, ρ_o (g/cm^3)
Al_2O_3	S		1.10	3.6		0.643	2.2	58.4/(Ref. 3)	0.25/(Ref. 48)	3.98
	P	1.06	1.12	5.4	0.657	0.659	0.30	61.2/(Ref. 3)	0.25/(Ref. 48)	3.98
SiC	S		1.16	5.5		0.730	7.7	58.2/(Ref. 3)	0.17/(Ref. 49)	3.22
	P	1.22	1.22	0.0	0.786	0.769	2.2	64.6/(Ref. 3)	0.17/(Ref. 49)	3.22
Si_3N_4	P	1.12	0.977	15.4	0.657	0.585	12.3	40.0/(Ref. 3)	0.22/(Ref. 3)	3.30
UO_2	S		0.558	1.4				33.4/(Ref. 3)	0.33/(Ref. 3)	10.69
	P	0.550	0.551	0.2				32.6/(Ref. 3)	0.33/(Ref. 3)	10.69
$YBa_2Cu_3O_{7-x}$	P	0.565	0.594	4.8	0.313	0.374	16.3	32.8/(Ref. 46)	0.27/(Ref. 11)	6.38
Steel	P	0.580	0.614	5.5				29.0/(Ref. 47)	0.33/(Ref. 47)	7.85
Tungsten	P	0.541	0.509	6.1				58.0/(Ref. 47)	0.27/(Ref. 47)	19.3

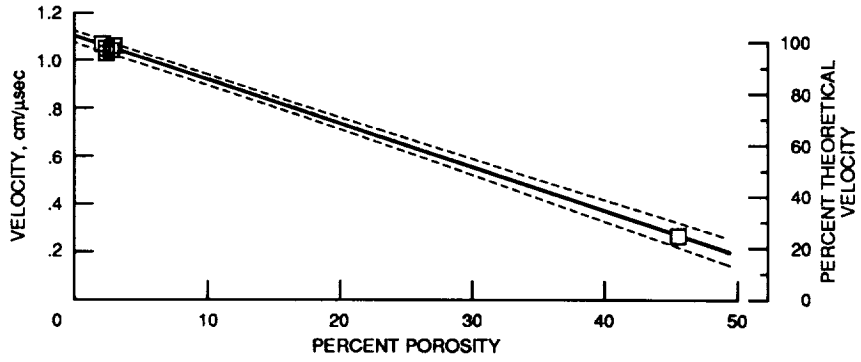

Figure 1. - Longitudinal velocity versus percent porosity for Al_2O_3 (ref. 24).
Velocity = –0.018 x percent porosity + 1.09.
Percent theoretical velocity = –1.65 x percent porosity + 100.
Correlation coefficient = –0.999.

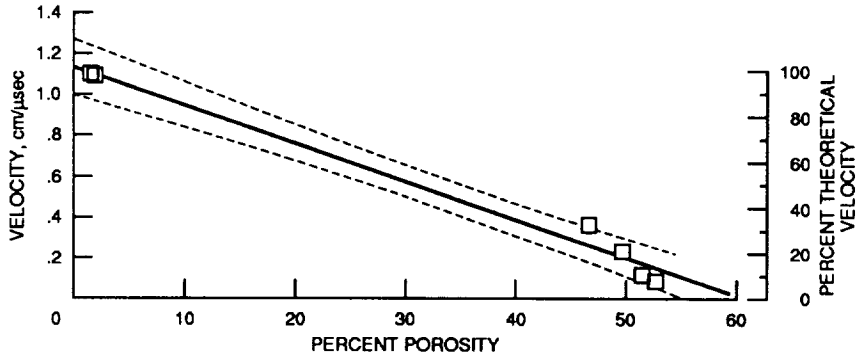

Figure 2. - Longitudinal velocity versus percent porosity for Al_2O_3 (ref. 25).
Velocity = –0.019 x percent porosity + 1.13.
Percent theoretical velocity = –1.64 x percent porosity + 100.
Correlation coefficient = –0.992.

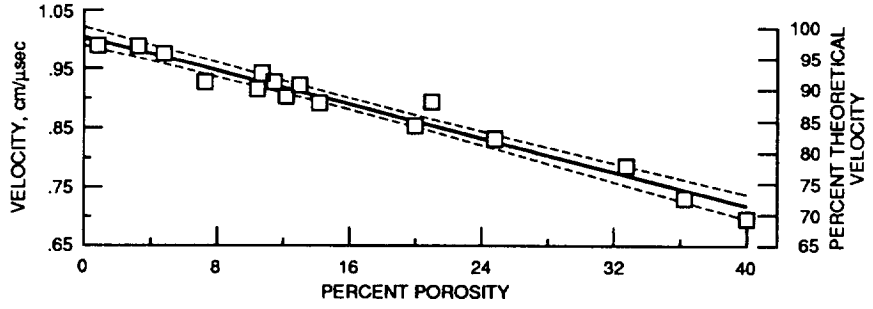

Figure 3. - Longitudinal velocity versus percent porosity for Al_2O_3 (ref. 16).
Velocity = –0.007 x percent porosity + 1.00.
Percent theoretical velocity = –0.736 x percent porosity + 100.
Correlation coefficient = –0.982.

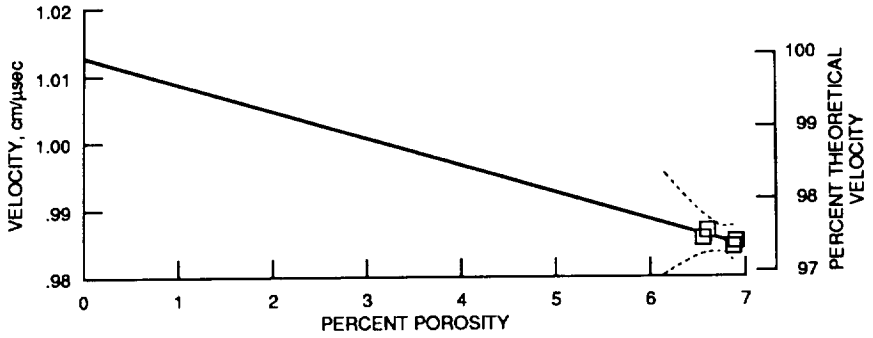

Figure 4. - Longitudinal velocity versus percent porosity for Al_2O_3 (ref. 26).
Velocity = –0.004 x percent porosity + 1.01.
Percent theoretical velocity = –0.377 x percent porosity + 100.
Correlation coefficient = –0.698.

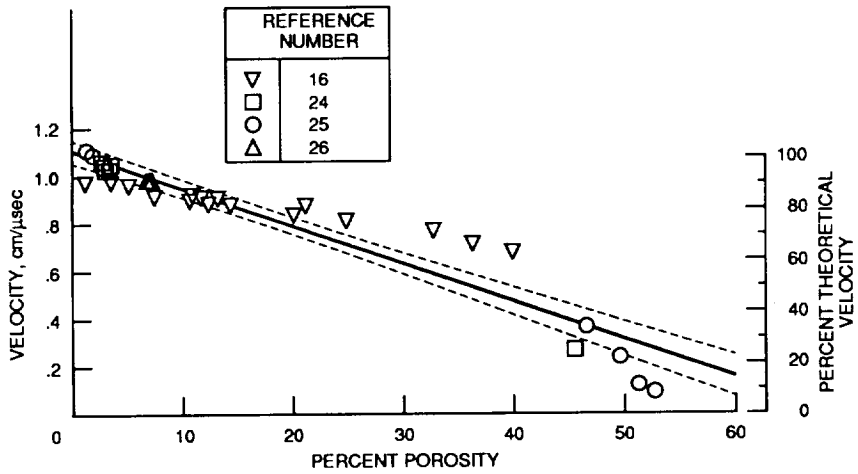

Figure 5. - Longitudinal velocity versus percent porosity for Al_2O_3 (refs. 16, 24 to 26).
Velocity = –0.016 x percent porosity + 1.10.
Percent theoretical velocity = –1.43 x percent porosity + 100.
Correlation coefficient = –0.949.

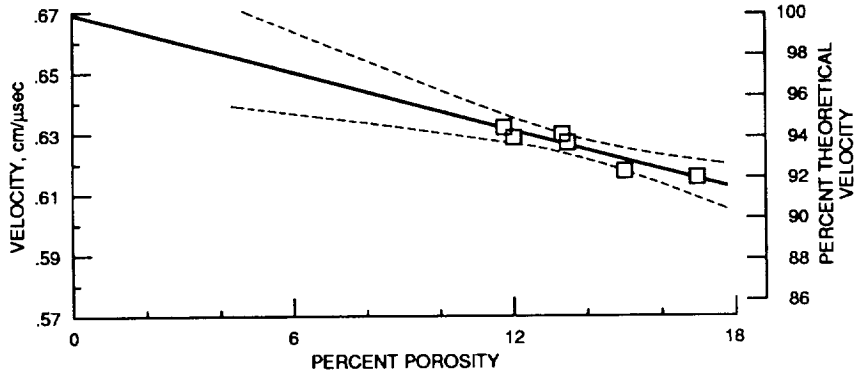

Figure 6. - Shear velocity versus percent porosity for Al_2O_3 (ref. 27).
Velocity = –0.003 x percent porosity + 0.669.
Percent theoretical velocity = –0.477 x percent porosity + 100.
Correlation coefficient = –0.936.

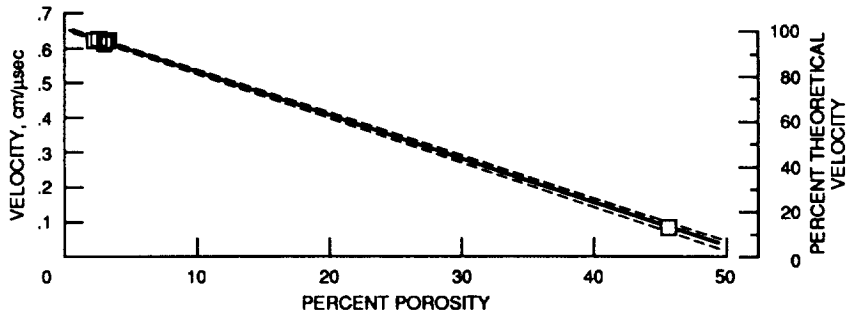

Figure 7. - Shear velocity versus percent porosity for Al_2O_3 (ref. 24).
Velocity = –0.012 x percent porosity + 0.655.
Percent theoretical velocity = –1.87 x percent porosity + 100.
Correlation coefficient = –1.00.

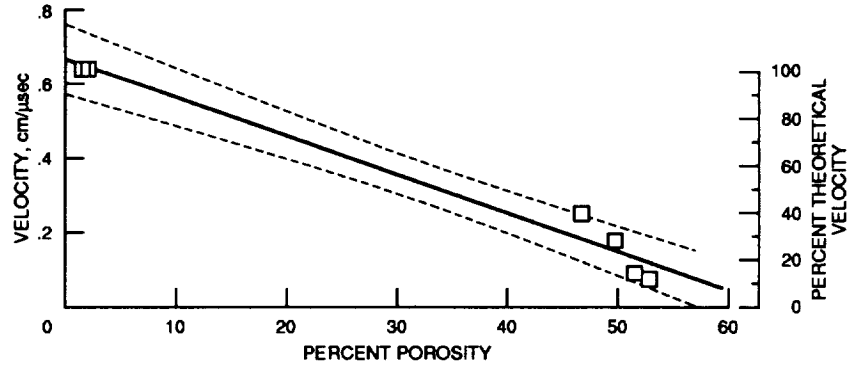

Figure 8. - Shear velocity versus percent porosity for Al_2O_3 (ref. 25).
Velocity = –0.010 x percent porosity + 0.666.
Percent theoretical velocity = –1.55 x percent porosity + 100.
Correlation coefficient = –0.987.

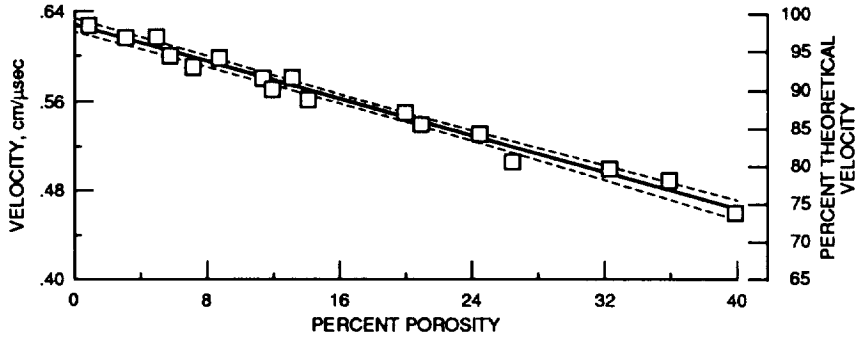

Figure 9. - Shear velocity versus percent porosity for Al_2O_3 (ref. 16).
Velocity = –0.004 x percent porosity + 0.628.
Percent theoretical velocity = –0.662 x percent porosity + 100.
Correlation coefficient = –0.990.

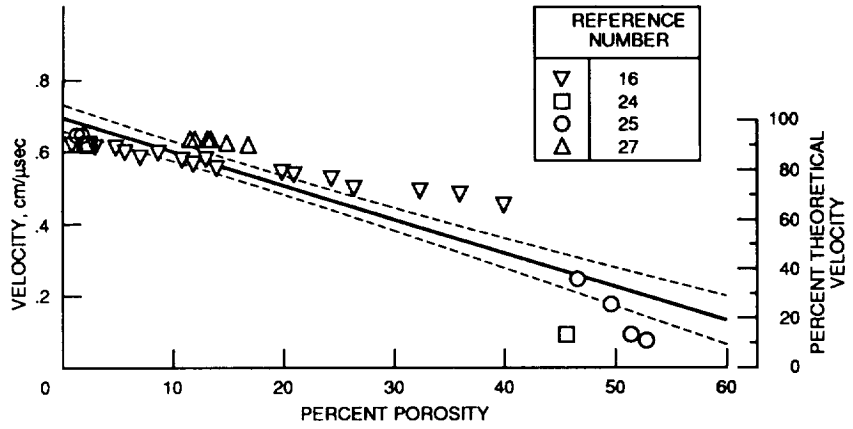

Figure 10. - Shear velocity versus percent porosity for Al_2O_3 (refs. 16, 24, 25, 27).
Velocity = –0.009 x percent porosity + 0.693.
Percent theoretical velocity = –1.35 x percent porosity + 100.
Correlation coefficient = –0.910.

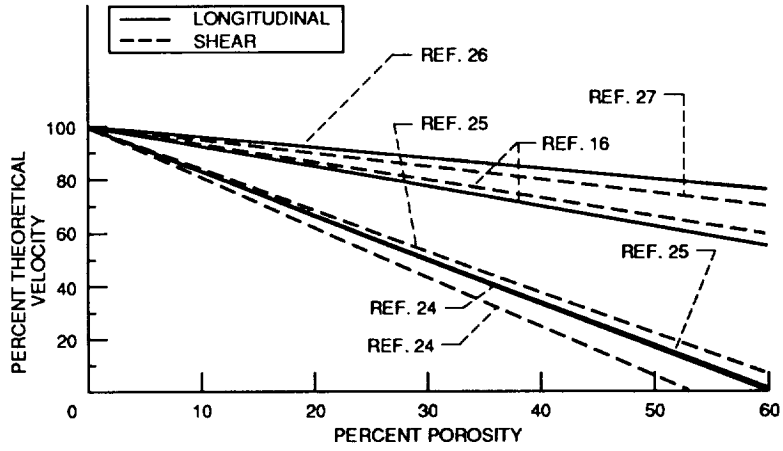

Figure 11. - Ultrasonic velocity versus percent porosity for Al_2O_3 (refs. 16, 24 to 27).

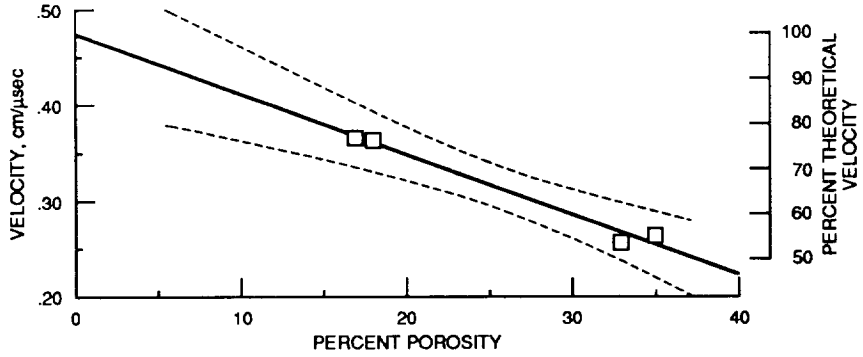

Figure 12. - Longitudinal velocity versus percent porosity for CuO (ref. 28).
Velocity = –0.006 x percent porosity + 0.474.
Percent theoretical velocity = –1.34 x percent porosity + 100.
Correlation coefficient = –0.990.

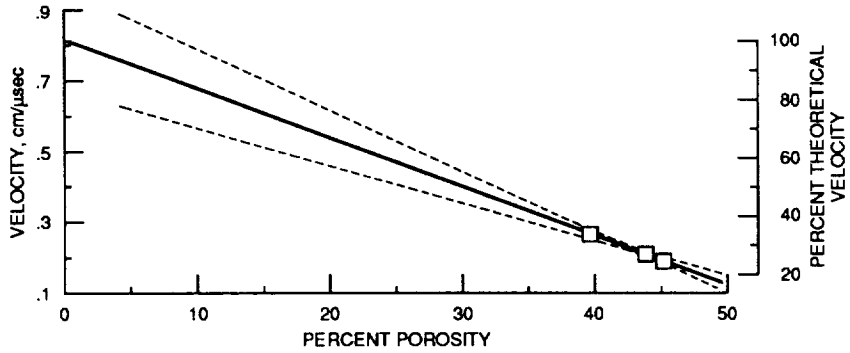

Figure 13. - Longitudinal velocity versus percent porosity for "green" M_gO (ref. 29).
Velocity = –0.018 x percent porosity + 0.817.
Correlation coefficient = –1.00.

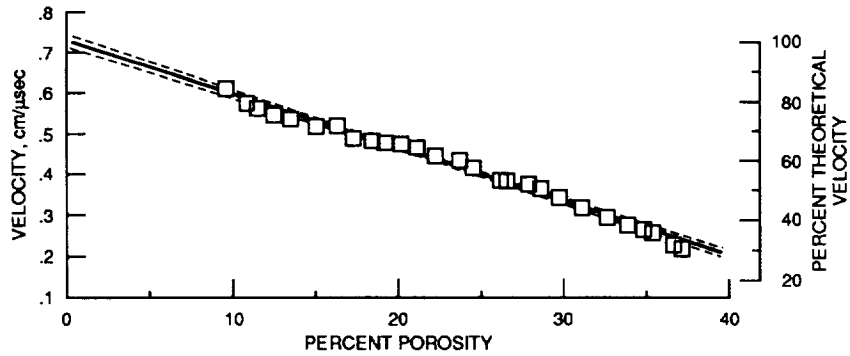

Figure 14. - Longitudinal velocity versus percent porosity for porcelain (ref. 7).
Velocity = –0.013 x percent porosity + 0.728.
Percent theoretical velocity = –1.78 x percent porosity + 100.
Correlation coefficient = –0.994.

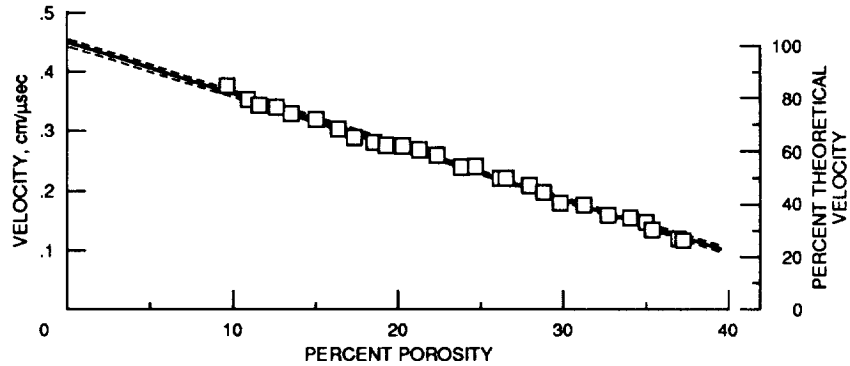

Figure 15. - Shear velocity versus percent porosity for porcelain (ref. 7).
Velocity = –0.009 x percent porosity + 0.448.
Percent theoretical velocity = –1.93 x percent porosity + 100.
Correlation coefficient = –0.998.

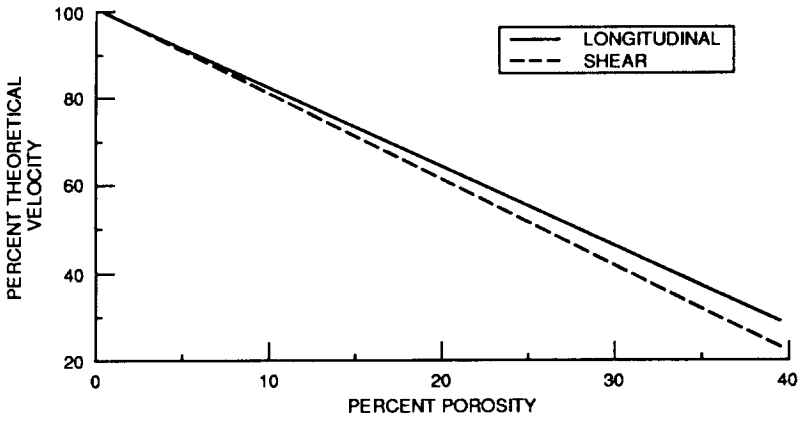

Figure 16. - Ultrasonic velocity versus percent porosity for porcelain (ref. 7).

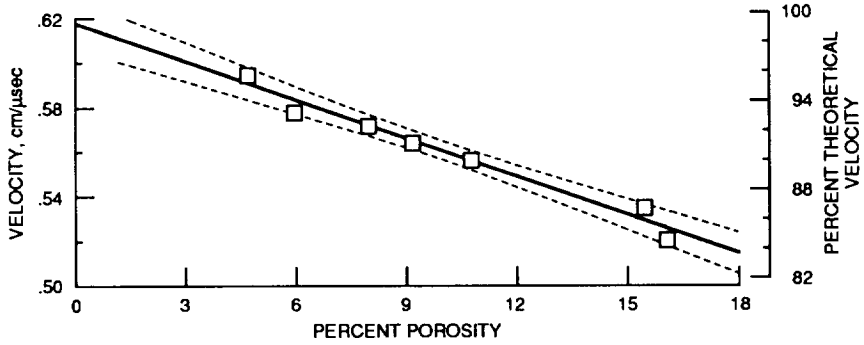

Figure 17. - Longitudinal velocity versus percent porosity for porcelain (ref. 30).
Velocity = –0.006 x percent porosity + 0.618.
Percent theoretical velocity = –0.935 x percent porosity + 100.
Correlation coefficient = –0.987.

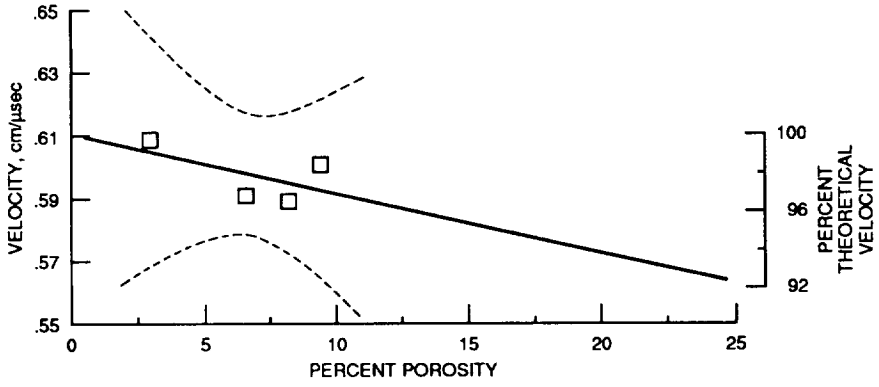

Figure 18. - Longitudinal velocity versus percent porosity for porcelain P1 (ref. 31).
Velocity = –0.002 x percent porosity + 0.611.
Percent theoretical velocity = –0.312 x percent porosity + 100.
Correlation coefficient = –0.586.

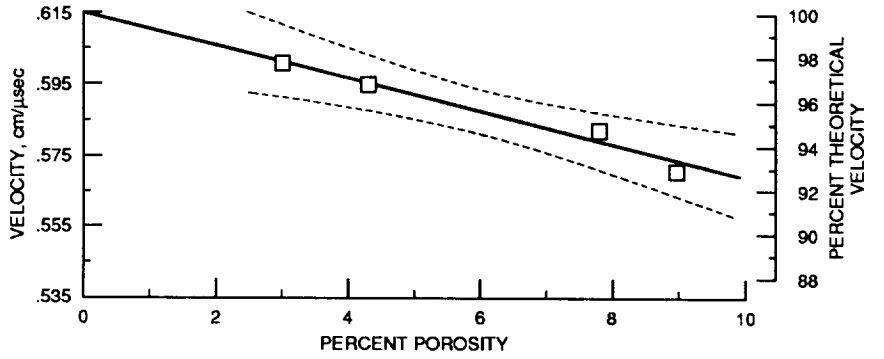

Figure 19. - Longitudinal velocity versus percent porosity for porcelain P2 (ref. 31).
Velocity = –0.005 x percent porosity + 0.615.
Percent theoretical velocity = –0.740 x percent porosity + 100.
Correlation coefficient = –0.983.

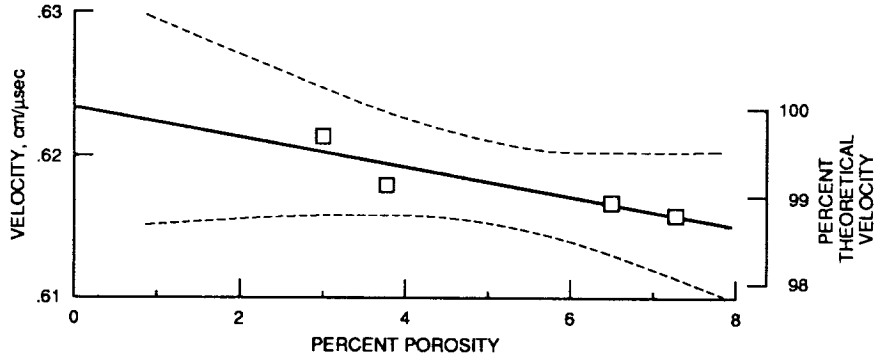

Figure 20. - Longitudinal velocity versus percent porosity for porcelain T1 (ref. 3).
Velocity = –0.001 x percent porosity + 0.623.
Percent theoretical velocity = –0.167 x percent porosity + 100.
Correlation coefficient = –0.894.

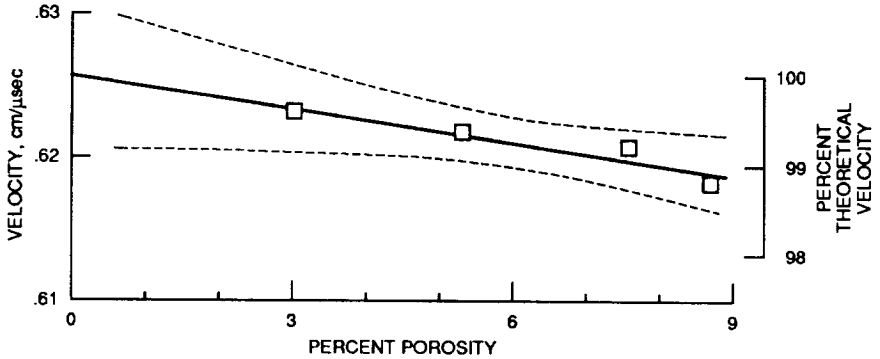

Figure 21. - Longitudinal velocity versus percent porosity for porcelain T2 (ref. 31).
Velocity = –0.001 x percent porosity + 0.626.
Percent theoretical velocity = –0.121 x percent porosity + 100.
Correlation coefficient = –0.947.

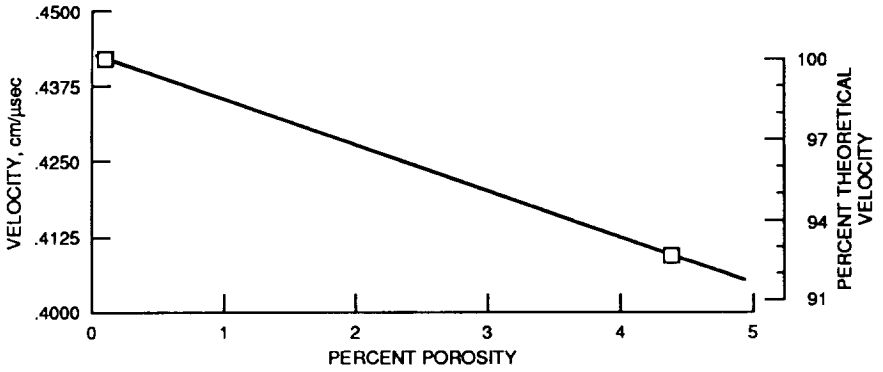

Figure 22. - Longitudinal velocity versus percent porosity for unpoled PZT4 (ref. 8).
Velocity = –0.007 x percent porosity + 0.443.
Percent theoretical velocity = –1.68 x percent porosity + 100.

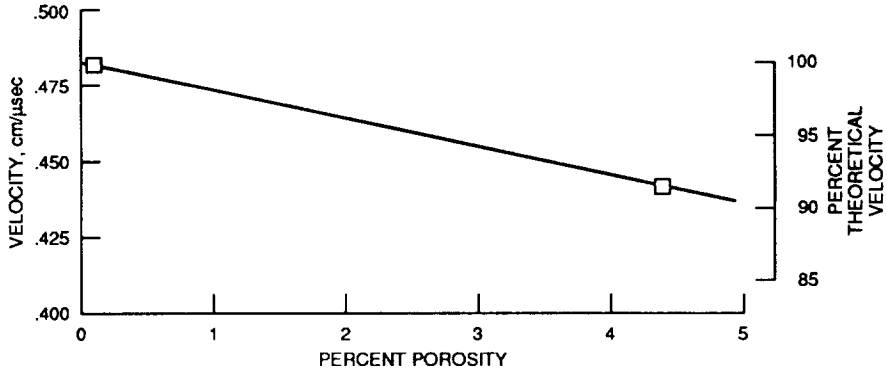

Figure 23. - Longitudinal velocity versus percent porosity for poled PZT4 (ref. 8).
Velocity = –0.009 x percent porosity + 0.483.
Percent theoretical velocity = –1.93 x percent porosity + 100.

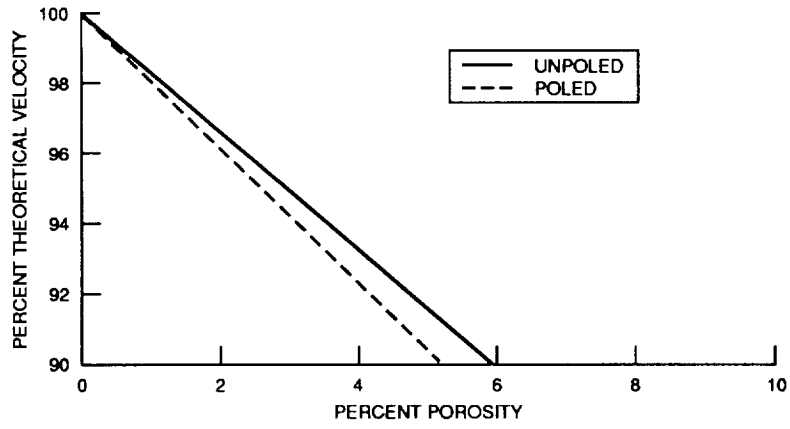

Figure 24. - Ultrasonic velocity versus percent porosity for PZT4 (ref. 8).

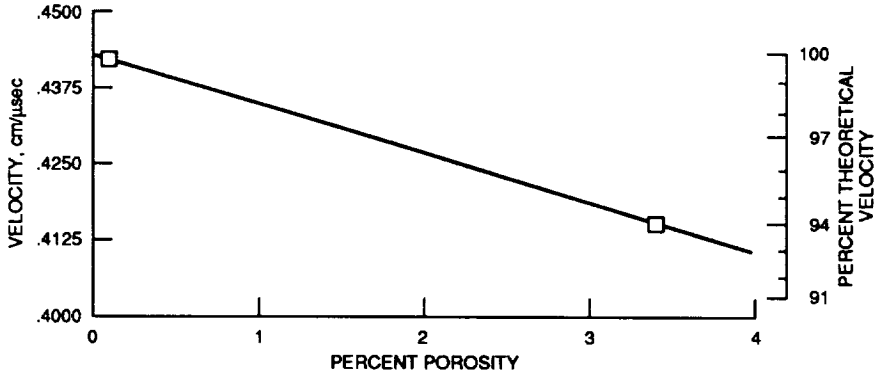

Figure 25. - Longitudinal velocity versus percent porosity for unpoled PZT5 (ref. 8).
Velocity = −0.008 x percent porosity + 0.443.
Percent theoretical velocity = −1.85 x percent porosity + 100.

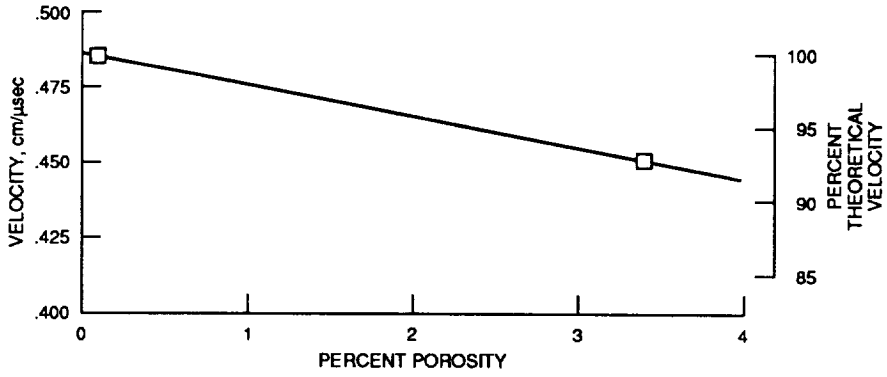

Figure 26. - Longitudinal velocity versus percent porosity for poled PZT5 (ref. 8).
Velocity = −0.010 x percent porosity + 0.486.
Percent theoretical velocity = −2.12 x percent porosity + 100.

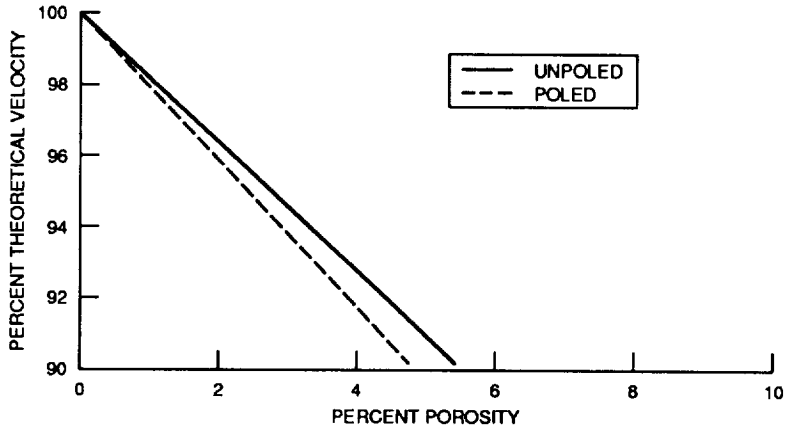

Figure 27. - Ultrasonic velocity versus percent porosity for PZT5 (ref. 8).

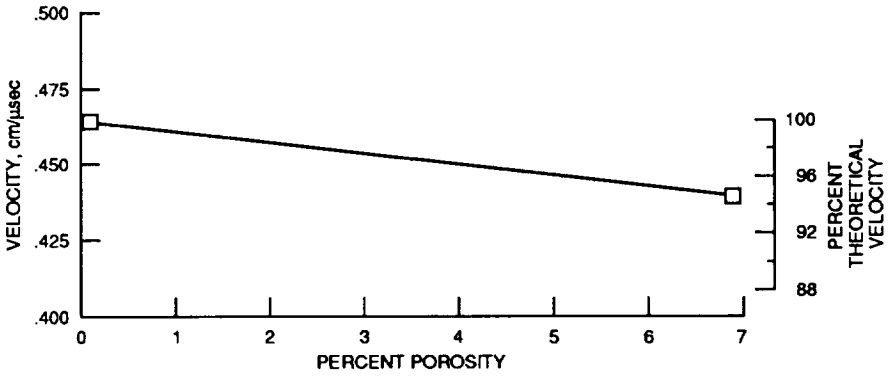

Figure 28. - Longitudinal velocity versus percent porosity for unpoled PZT7 (ref. 8).
Velocity = –0.004 x percent porosity + 0.464.
Percent theoretical velocity = –0.760 x percent porosity + 100.

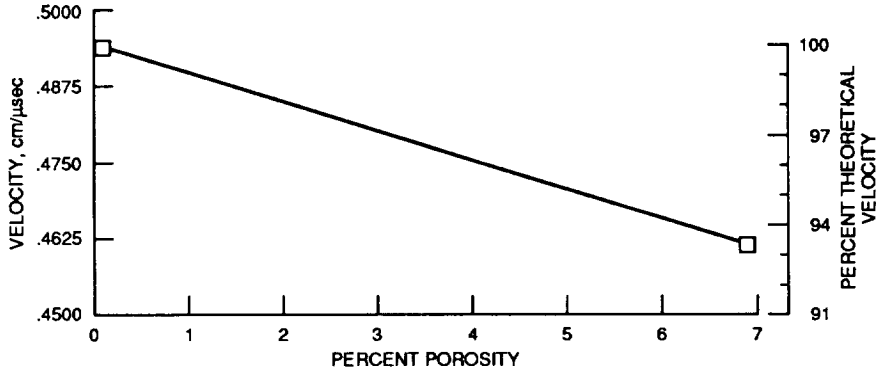

Figure 29. - Longitudinal velocity versus percent porosity for poled PZT7 (ref. 8).
Velocity = –0.005 x percent porosity + 0.494.
Percent theoretical velocity = –0.952 x percent porosity + 100.

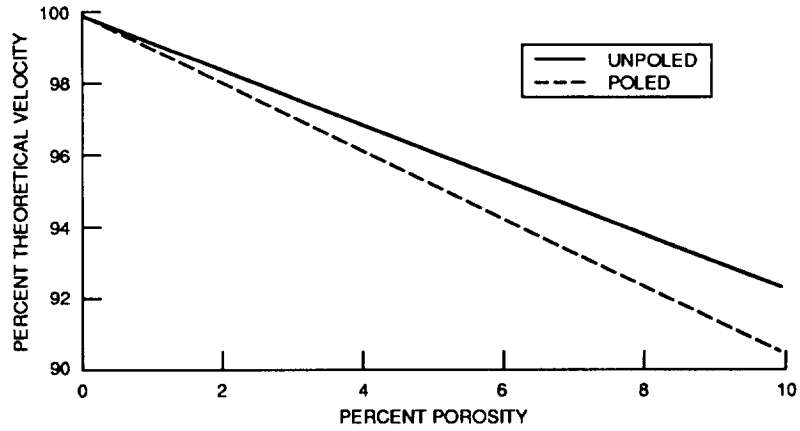

Figure 30. - Ultrasonic velocity versus percent porosity for PZT7 (ref. 8).

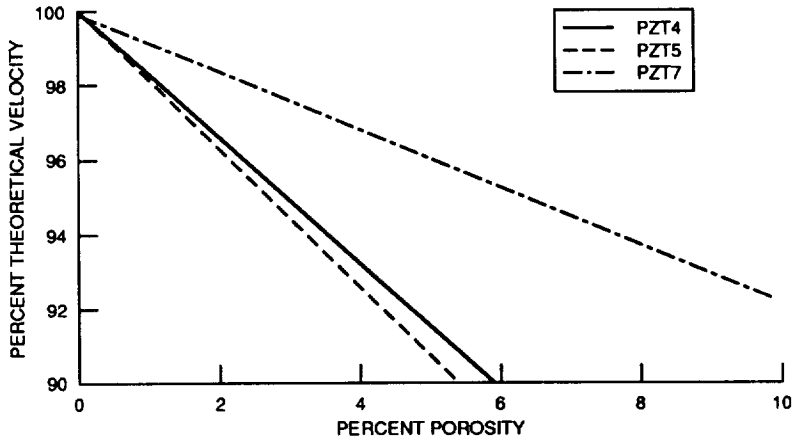

Figure 31. - Ultrasonic velocity versus percent porosity for unpoled PZT (ref. 8).

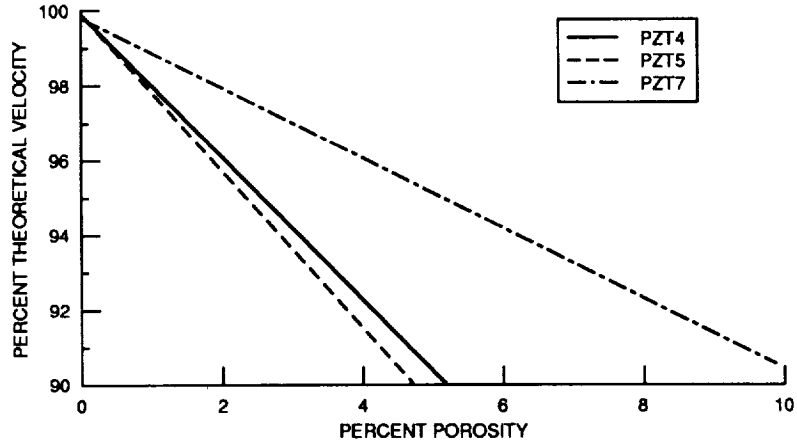

Figure 32. - Ultrasonic velocity versus percent porosity for poled PZT (ref. 8).

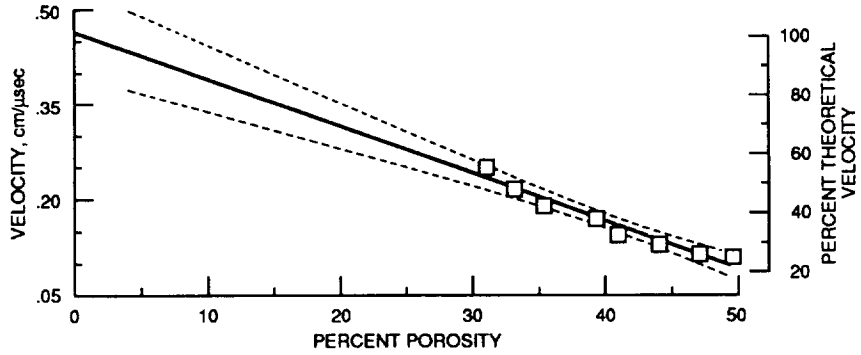

Figure 33. - Longitudinal velocity versus percent porosity for green SiC (ref. 32).
Velocity = –0.007 x percent porosity + 0.464.
Correlation coefficient = –0.974.

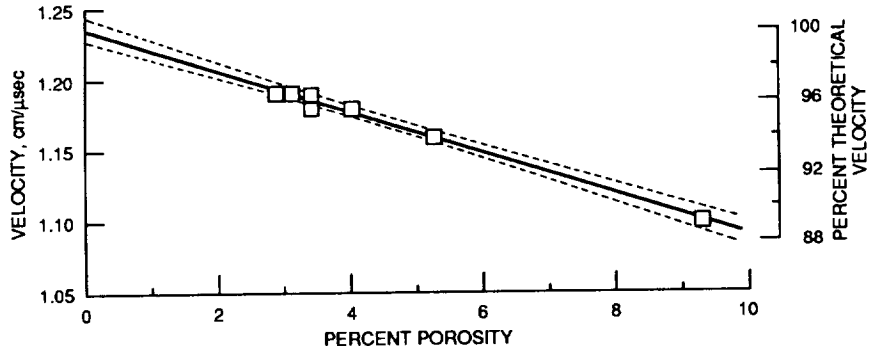

Figure 34. - Longitudinal velocity versus percent porosity for SiC (ref. 33).
Velocity = –0.014 x percent porosity + 1.23.
Percent theoretical velocity = –1.16 x percent porosity + 100.
Correlation coefficient = –0.993.

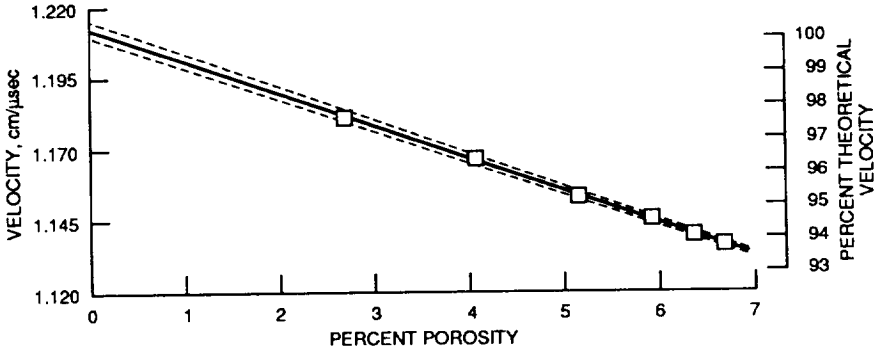

Figure 35. - Longitudinal velocity versus percent porosity for SiC (ref. 34).
Velocity = –0.011 x percent porosity + 1.21.
Percent theoretical velocity = –0.916 x percent porosity + 100.
Correlation coefficient = –0.999.

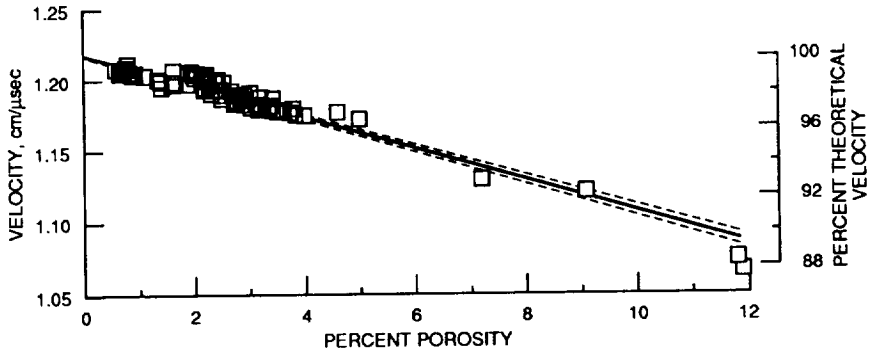

Figure 36. - Longitudinal velocity versus percent porosity for SiC (ref. 35).
Velocity = –0.011 x percent porosity + 1.22.
Percent theoretical velocity = –0.883 x percent porosity + 100.
Correlation coefficient = –0.957.

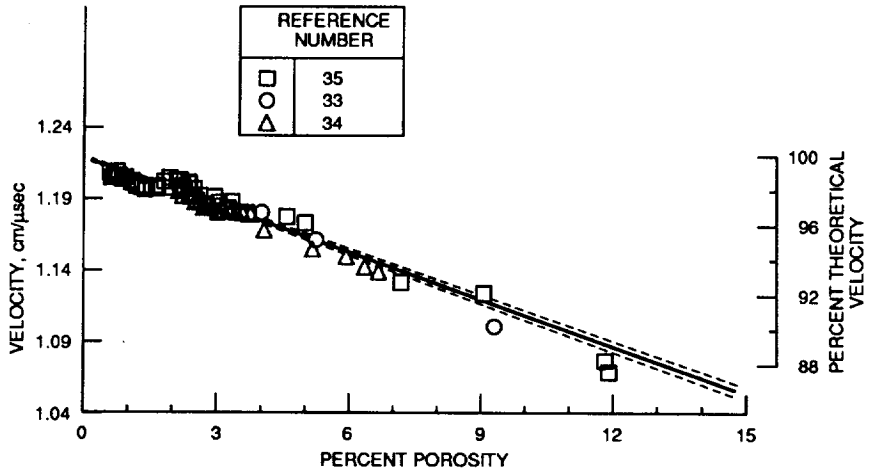

Figure 37. - Longitudinal velocity versus percent porosity for SiC (refs. 33 to 35).
Velocity = –0.011 x percent porosity + 1.22.
Percent theoretical velocity = –0.912 x percent porosity + 100.
Correlation coefficient = –0.964.

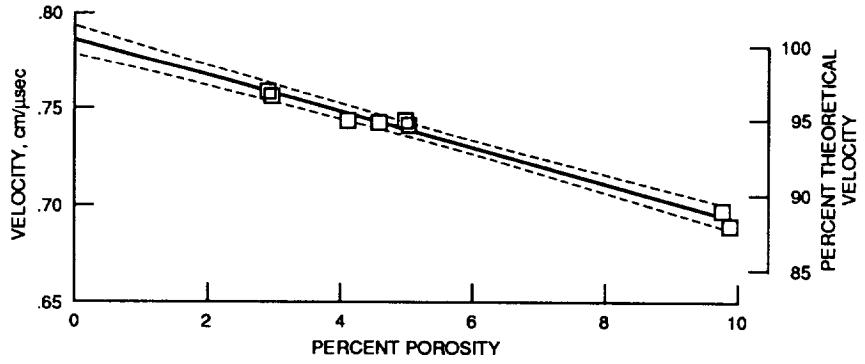

Figure 38. - Shear velocity versus percent porosity for SiC (ref. 26).
Velocity = –0.009 x percent porosity + 0.786.
Percent theoretical velocity = –1.16 x percent porosity + 100.
Correlation coefficient = –0.991.

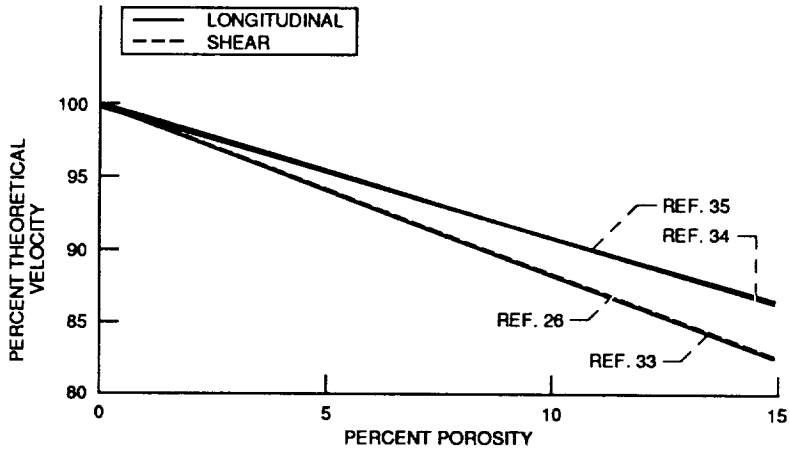

Figure 39. - Ultrasonic velocity versus percent porosity for SiC (refs. 26, 33 to 35).

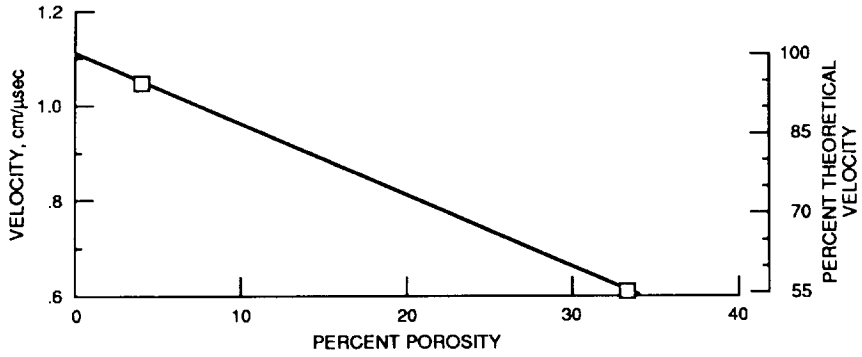

Figure 40. - Longitudinal velocity versus percent porosity for Si_3N_4 (ref. 36).
Velocity = –0.015 x percent porosity + 1.11.
Percent theoretical velocity = –1.34 x percent porosity + 100.

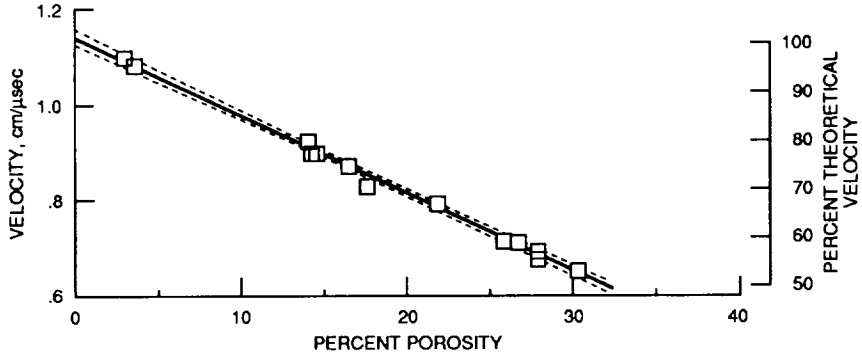

Figure 41. - Longitudinal velocity versus percent porosity for Si_3N_4 (ref. 37).
Velocity = –0.016 x percent porosity + 1.14.
Percent theoretical velocity = –1.41 x percent porosity + 100
Correlation coefficient = –0.997.

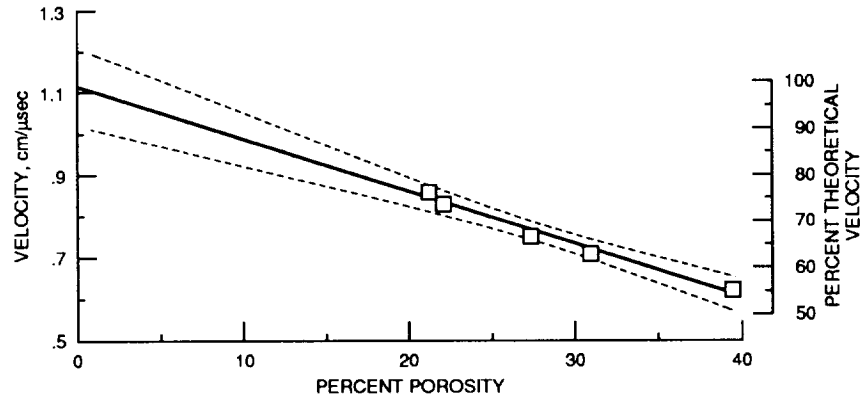

Figure 42. - Longitudinal velocity versus percent porosity for Si_3N_4 (ref. 38).
Velocity = –0.013 x percent porosity + 1.12.
Percent theoretical velocity = –1.15 x percent porosity + 100
Correlation coefficient = –0.991.

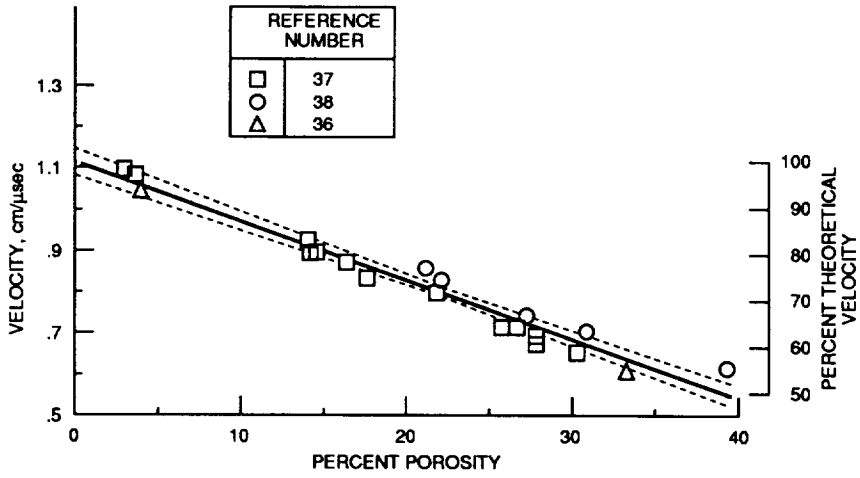

Figure 43. - Longitudinal velocity versus percent porosity for Si_3N_4 (refs. 36 to 38).
Velocity = –0.014 x percent porosity + 1.12.
Percent theoretical velocity = –1.27 x percent porosity + 100
Correlation coefficient = –0.981.

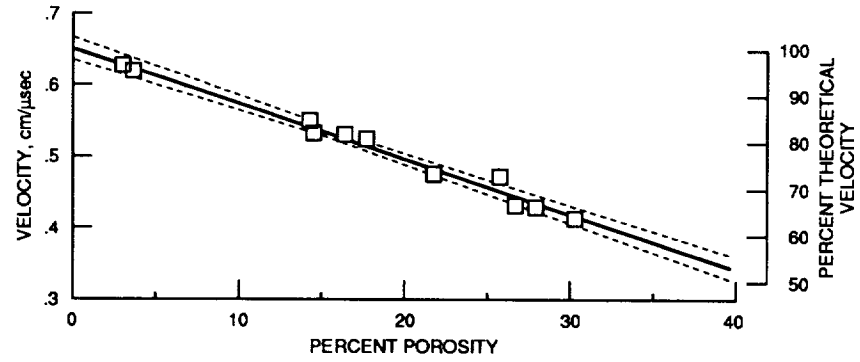

Figure 44. - Shear velocity versus percent porosity for Si_3N_4 (ref. 37).
Velocity = –0.008 x percent porosity + 0.652.
Percent theoretical velocity = –1.18 x percent porosity + 100
Correlation coefficient = –0.991.

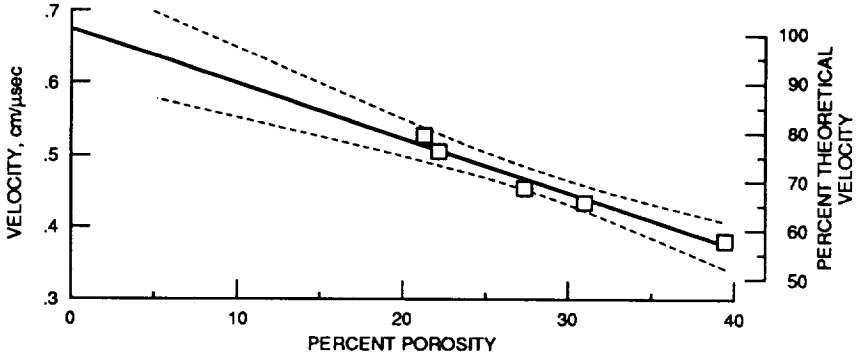

Figure 45. - Shear velocity versus percent porosity for Si_3N_4 (ref. 38).
Velocity = –0.007 x percent porosity + 0.675.
Percent theoretical velocity = –1.10 x percent porosity + 100
Correlation coefficient = –0.984.

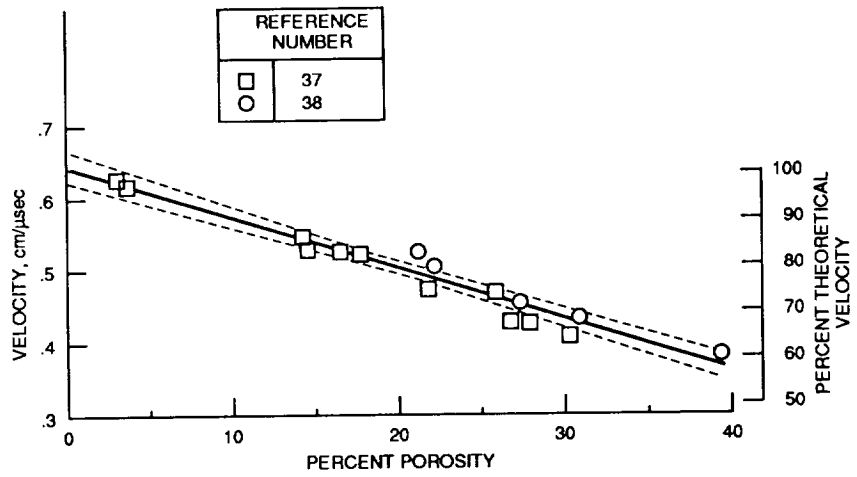

Figure 46. - Shear velocity versus percent porosity for Si_3N_4 (refs. 37, 38).
Velocity = –0.007 x percent porosity + 0.645.
Percent theoretical velocity = –1.07 x percent porosity + 100
Correlation coefficient = –0.973.

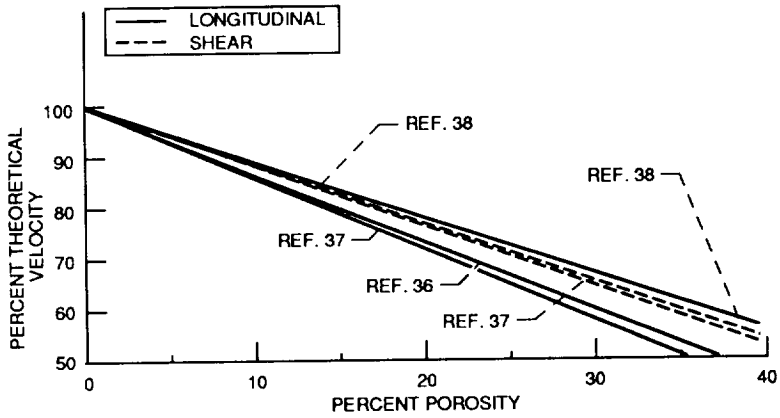

Figure 47. - Ultrasonic velocity versus percent porosity for Si_3N_4 (refs. 36 to 38).

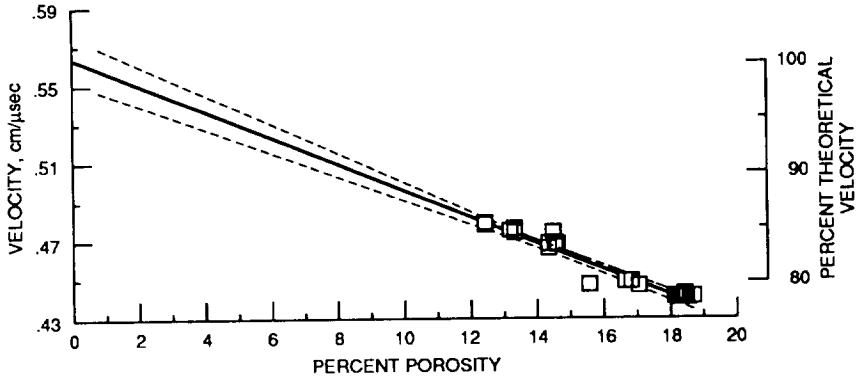

Figure 48. - Longitudinal velocity measured in the A direction versus percent porosity for steel (ref. 39).
Velocity = –0.007 x percent porosity + 0.563.
Percent theoretical velocity = –1.19 x percent porosity + 100.
Correlation coefficient = –0.972.

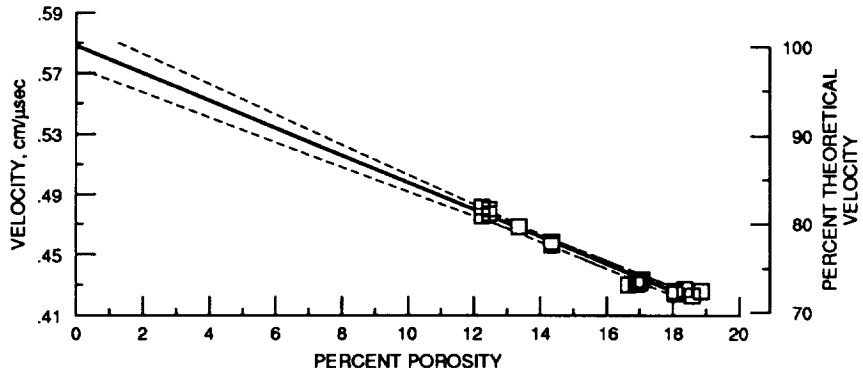

Figure 49. - Longitudinal velocity measured in the B direction versus percent porosity for steel (ref. 39).
Velocity = −0.009 x percent porosity + 0.588.
Percent theoretical velocity = −1.53 x percent porosity + 100.
Correlation coefficient = −0.985.

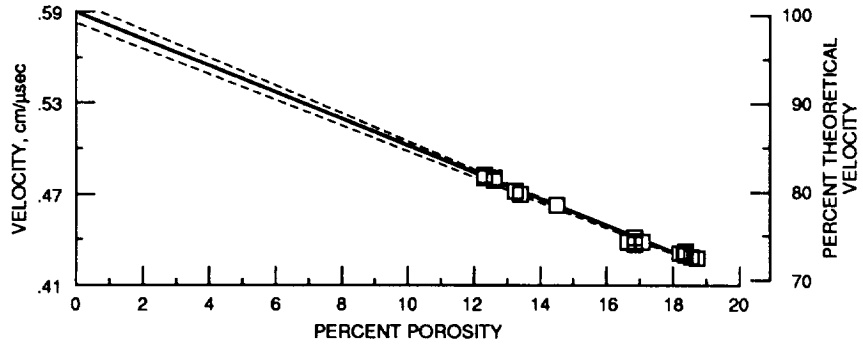

Figure 50. - Longitudinal velocity measured in the C direction versus percent porosity for steel (ref. 39).
Velocity = −0.009 x percent porosity + 0.590.
Percent theoretical velocity = −1.48 x percent porosity + 100.
Correlation coefficient = −0.996.

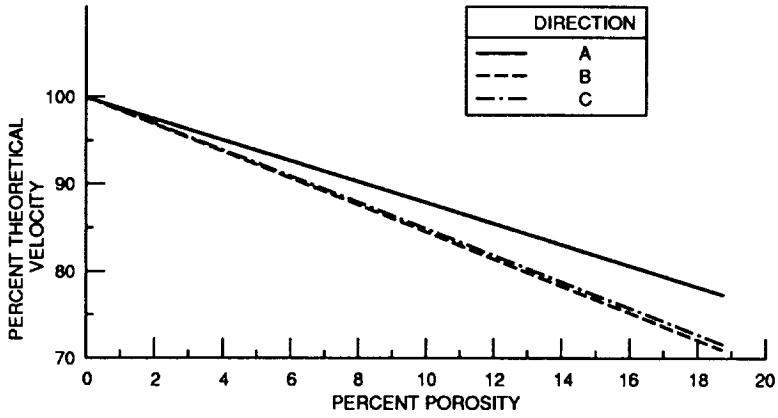

Figure 51. - Ultrasonic velocity versus percent porosity for steel (ref. 39).

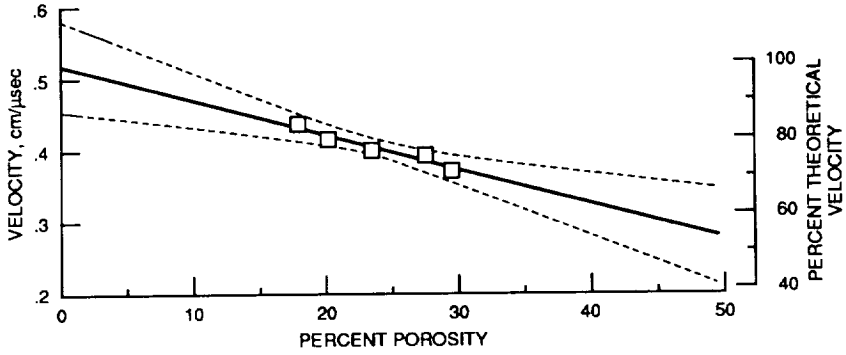

Figure 52. - Longitudinal velocity versus percent porosity for tungsten (ref. 2) with Kenna nominal 4 μm starting powder size.
Velocity = –0.005 x percent porosity + 0.520.
Percent theoretical velocity = –0.939 x percent porosity + 100.
Correlation coefficient = –0.960.

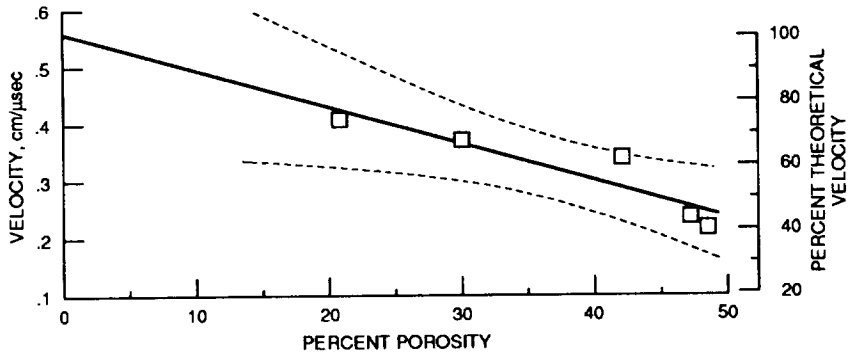

Figure 53. - Longitudinal velocity versus percent porosity for tungsten (ref. 2) with General Electric nominal 4 μm starting powder size.
Velocity = –0.006 x percent porosity + 0.558.
Percent theoretical velocity = –1.13 x percent porosity + 100.
Correlation coefficient = –0.918.

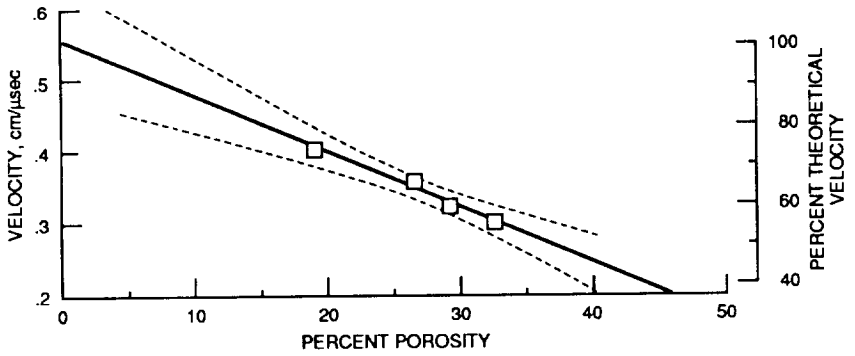

Figure 54. - Longitudinal velocity versus percent porosity for tungsten (ref. 2) with General Electric nominal 18 μm starting powder size.
Velocity = –0.008 x percent porosity + 0.554.
Percent theoretical velocity = –1.38 x percent porosity + 100.
Correlation coefficient = –0.992.

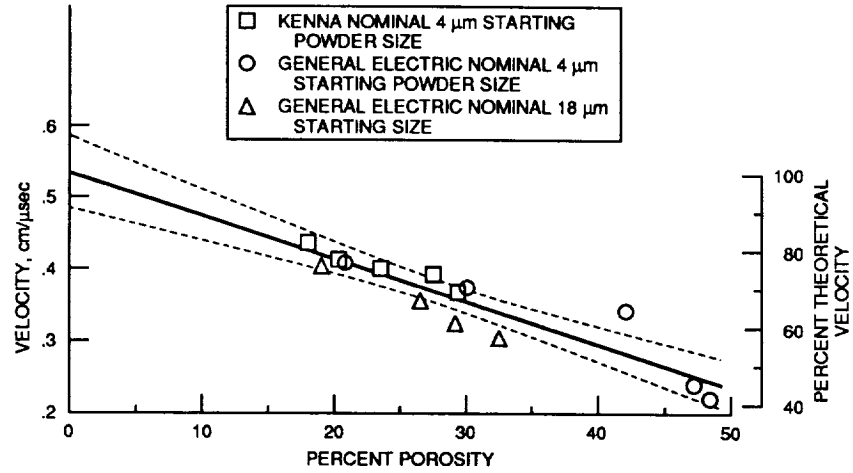

Figure 55. - Longitudinal velocity versus percent porosity for tungsten (ref. 2).
Velocity = –0.006 x percent porosity + 0.533.
Percent theoretical velocity = –1.11 x percent porosity + 100.
Correlation coefficient = –0.916.

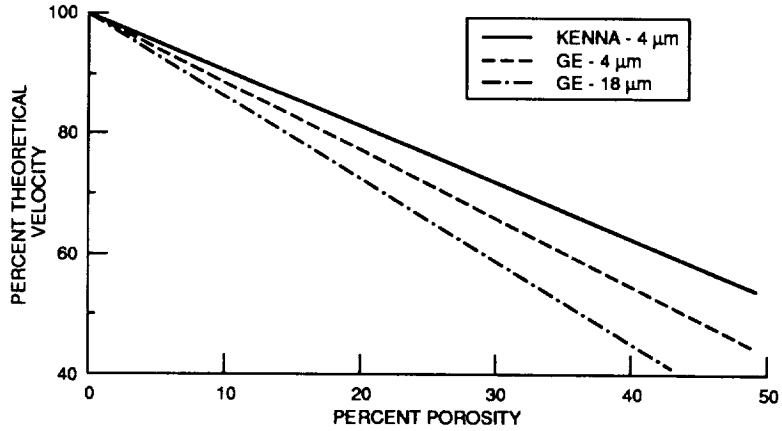

Figure 56. - Longitudinal velocity versus percent porosity for tungsten (ref. 2).

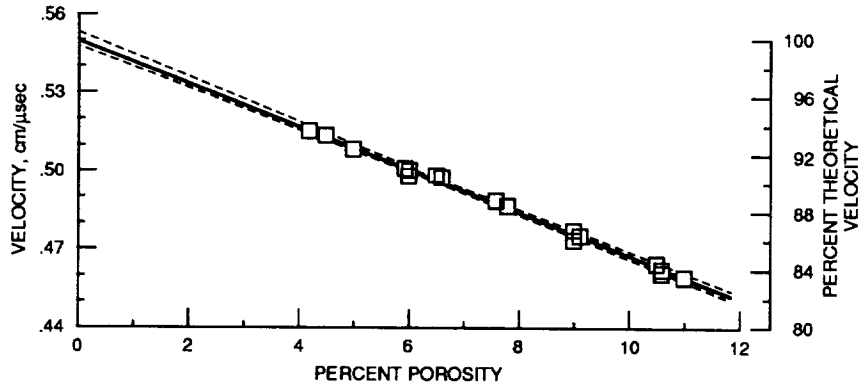

Figure 57. - Longitudinal velocity versus percent porosity for UO_2 (ref. 40).
Velocity = –0.008 x percent porosity + 0.550.
Percent theoretical velocity = –1.49 x percent porosity + 100.
Correlation coefficient = –0.997.

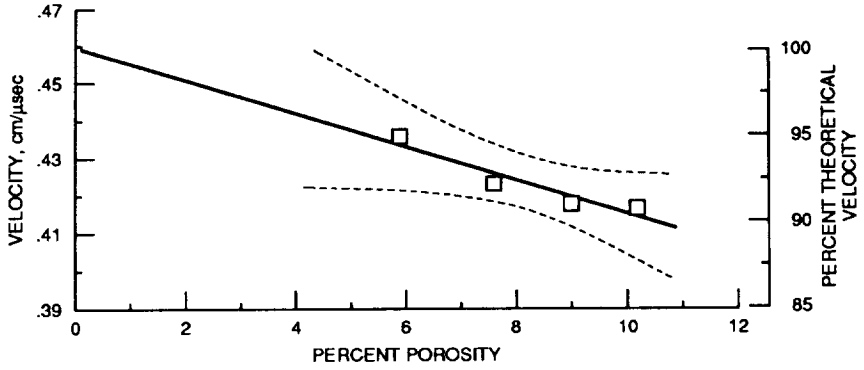

Figure 58. - Longitudinal velocity versus percent porosity for $(U_{0.30}Pu_{0.70})C$ (ref. 41).
Velocity = –0.004 x percent porosity + 0.460.
Percent theoretical velocity = –0.958 x percent porosity + 100.
Correlation coefficient = –0.949.

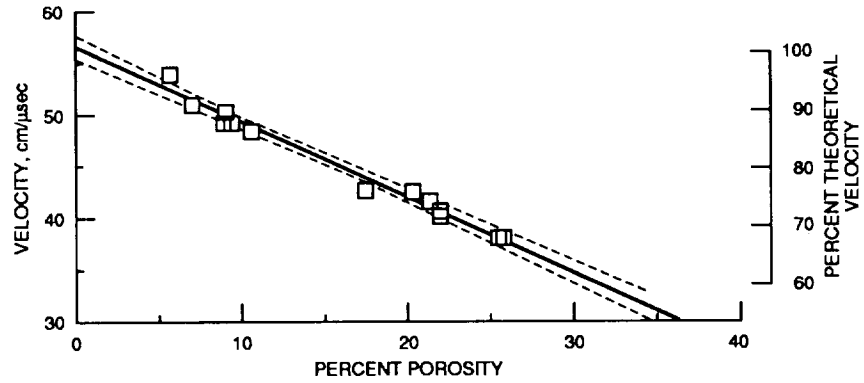

Figure 59. - Longitudinal velocity versus percent porosity for $YBa_2Cu_3O_{7-x}$ (ref. 43).
Velocity = –0.007 x percent porosity + 0.565.
Percent theoretical velocity = –1.28 x percent porosity + 100.
Correlation coefficient = –0.991.

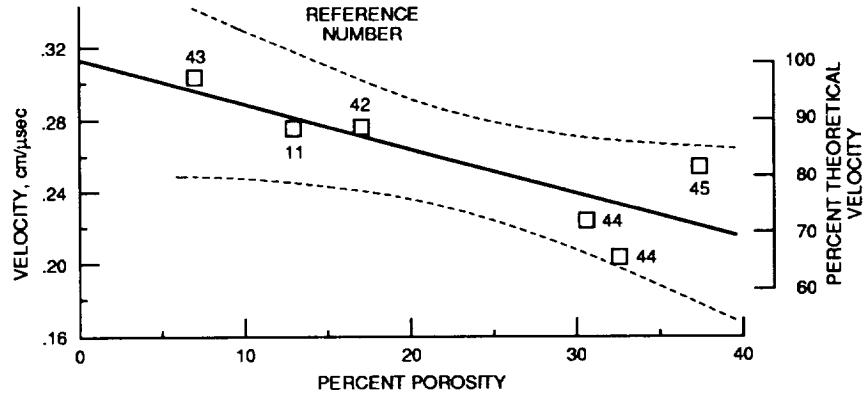

Figure 60. - Shear velocity versus percent porosity for $YBa_2Cu_3O_{7-x}$ (refs. 11, 42 to 45).
Velocity = –0.002 x percent porosity + 0.313.
Percent theoretical velocity = –0.768 x percent porosity + 100.
Correlation coefficient = –0.814.

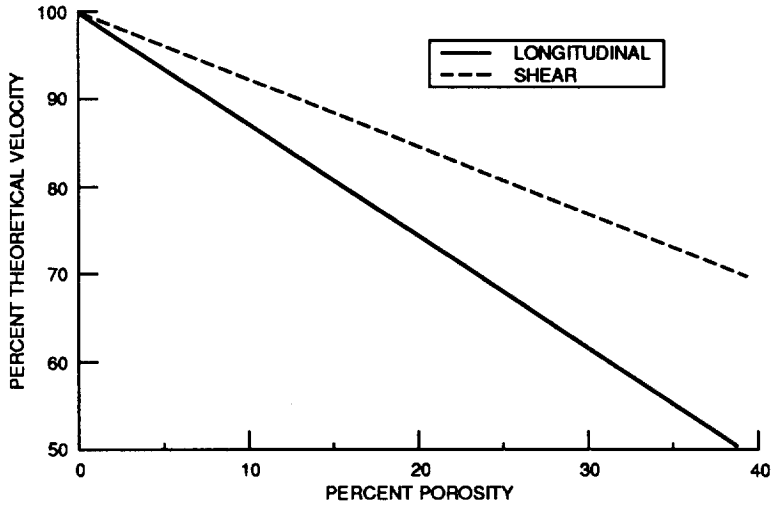

Figure 61. - Ultrasonic velocity versus percent porosity for $YBa_2Cu_3O_{7-x}$ (refs 11, 42 to 45).

NASA
National Aeronautics and Space Administration

Report Documentation Page

1. Report No.	2. Government Accession No.	3. Recipient's Catalog No.
NASA TM-102501 Revised Copy		

4. Title and Subtitle

Review and Statistical Analysis of the Ultrasonic Velocity Method for Estimating the Porosity Fraction in Polycrystalline Materials

5. Report Date

July 1990

6. Performing Organization Code

7. Author(s)

D.J. Roth, D.B. Stang, S.M. Swickard, M.R DeGuire

8. Performing Organization Report No.

E-5298

10. Work Unit No.

506-43-11

9. Performing Organization Name and Address

National Aeronautics and Space Administration
Lewis Research Center
Cleveland, Ohio 44135-3191

11. Contract or Grant No.

13. Type of Report and Period Covered

Technical Memorandum

12. Sponsoring Agency Name and Address

National Aeronautics and Space Administration
Washington, D.C. 20546-0001

14. Sponsoring Agency Code

15. Supplementary Notes

D.J. Roth and S.M. Swickard, NASA Lewis Research Center. D.B. Stang, Sverdrup Technology, Inc., Lewis Research Center Group, 2001 Aerospace Parkway, Brook Park, Ohio 44142. M.R. DeGuire, Case Western Reserve University, Cleveland, Ohio 44106.

16. Abstract

A review and statistical analysis of the ultrasonic velocity method for estimating the porosity fraction in polycrystalline materials is presented. Initially, a semi-empirical model is developed showing the origin of the linear relationship between ultrasonic velocity and porosity fraction. Then, from a compilation of data produced by many researchers, scatter plots of velocity versus percent porosity data are shown for Al_2O_3, CuO, MgO, porcelain-based ceramics, PZT, SiC, Si_3N_4, steel, tungsten, UO_2, $(U_{0.30}Pu_{0.70})C$, and $YBa_2Cu_3O_{7-x}$. Linear regression analysis produced predicted slope, intercept, correlation coefficient, level of significance, and confidence interval statistics for the data. Velocity values predicted from regression analysis for fully-dense materials are in good agreement with those calculated from elastic properties.

17. Key Words (Suggested by Author(s))	18. Distribution Statement
Ultrasonics; Ultrasonic velocity; Density; Porosity; Microstructure porosity fraction; Ceramics; Metals; Polycrystalline materials	Unclassified – Unlimited Subject Category 38

19. Security Classif. (of this report)	20. Security Classif. (of this page)	21. No. of pages	22. Price*
Unclassified	Unclassified	46	A03

NASA FORM 1626 OCT 86

*For sale by the National Technical Information Service, Springfield, Virginia 22161